Chapter 2:

Multifunctional Role of KISS1 in Regulating Transcription, EMT, and Apoptosis in Triple-Negative Breast Cancer: A Pleotropic effect

INTRODUCTION

Breast cancer is the most frequently diagnosed cancer and the foremost cause of cancer-related death in females. With approximate global cancer statistics, breast cancer accounts for nearly a quarter of all female cancers and millions of breast cancer incidence is diagnosed each year. With the most effective breakthroughs in the detection and treatment of breast cancer through surgical approaches, radiation therapy, chemotherapy, hormone therapy, and targeted therapies, it continues to be a significant clinical problem due to its heterogeneity and unpredictability. This leads to diversity of treatment responses, rates of recurrence, metastasis, and survival rates. (Liu et al., 2025).

Breast cancer was once regarded as a single disease entity; rather, it is a composition of molecularly distinct subtypes that carry distinct genetic, transcriptional, and metabolic profiles. Molecular classification according to hormone receptor status and gene expression profiling has thus far permitted an improved stratification of patients and therapeutic precision. Not all breast cancer subtypes have benefited from these advances in equal measure. Among them, Triple-Negative Breast Cancer represents one of the most aggressive and therapeutically challenging forms of the disease (Fultang et al., 2021; Guo et al., 2024).

TNBC is characterized by the absence of estrogen receptor (ER), progesterone receptor (PR), and human epidermal growth factor receptor 2 (HER2) expression. Consequently, these receptor-negative profiles make these patients unsuitable for hormone-targeted therapies such as tamoxifen or aromatase inhibitors and HER2-specific therapies such as trastuzumab, leaving cytotoxic chemotherapy as the main available systemic therapeutic approach. Despite the initial sensitivity of TNBC to chemotherapeutic agents, resistance rapidly develops, resulting in early relapse, high metastatic burden, and shortened overall survival rate. In terms of clinical profiles, TNBC is distinguished by its higher tumor grade, higher proliferation rate, early onset of visceral metastasis, and shorter disease-free survival than those of other breast cancer subtypes.(Jørgensen et al., 2020; Kepuladze et al., 2024) (Figure 2.1).

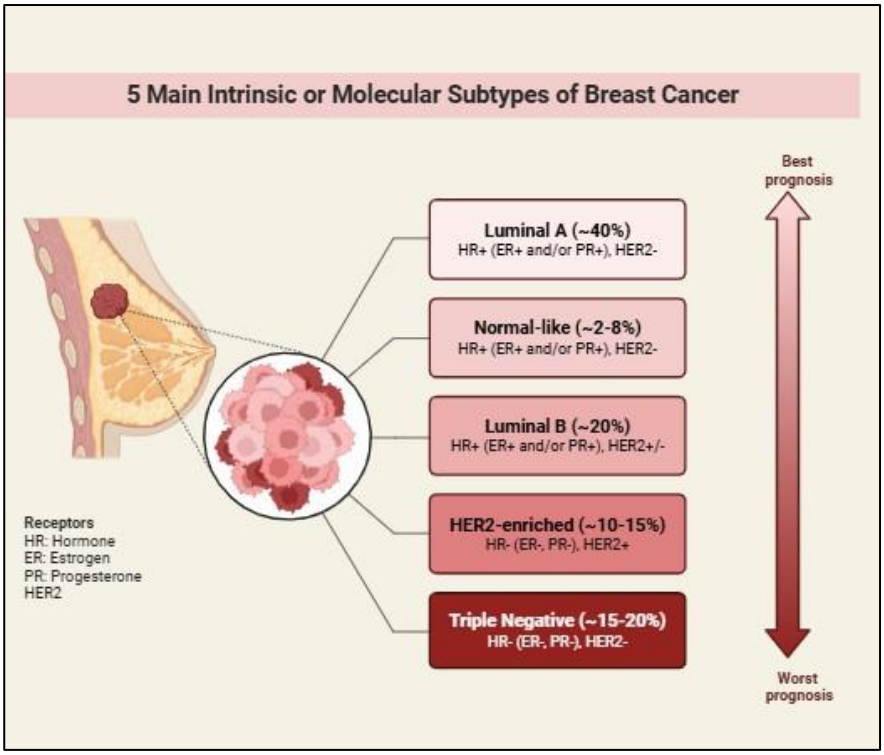

Figure 2.1: *Molecular Subtypes of Breast Cancer*

TNBC tends to be very aggressive, primarily occuring in younger premenopausal females. It has been shown to be more prevalent among females of African descent. The statistics have further emphasized the aggressiveness of TNBC, in addition to its immense socioeconomic significance. The unavailability of predictive biomarkers makes it even more urgent to look for new molecular modulators for the management of TNBC (Rios Garcia et al., 2017; Ulm et al., 2019). Biologically, at a molecular level, TNBC is known to exhibit a high degree of genetic heterogeneity, transcriptional heterogeneity, and metabolic heterogeneity. Several large-scale analyses of gene expression profiling experiments have identified distinct subtypes of TNBC by which they can be classified into basal-like subtype, mesenchymal-like subtype, immunomodulatory subtype, and the luminal androgen receptor (LAR) subtype of TNBC, among others.(Scheiber et al., 2014; Shan et al., 2017).

Of these, basal-like and mesenchymal-like are the most aggressive subgroups of TNBC. Basal-like TNBC is characterized by an enrichment of DNA damage repair, proliferation, whereas mesenchymal-like TNBC is marked by an increase in EMT, stemness, invasiveness, and chemotherapy resistance. EMT is a biological phenomenon that results from the loss of polarity and cell adhesion of epithelial cells, which then take on mesenchymal features, thereby promoting migration, invasions, and metastasis. During EMT, there is a loss of adhesion proteins like E-cadherin, whereas there is an induction of mesenchymal markers like N-cadherin, Vimentin, and CD44, along with the induction of a transcriptional suppressor like ZEB1.(Drápela et al., 2020; Usman et al., 2021; Zhang et al., 2019).

The aggressive nature of TNBC is driven by a multitude of cellular processes, including the disruption of transcription factors, oncogenic signaling, adhesion, resistance to apoptosis, and the disruption of cellular metabolism. Transcriptional targets for various therapies include SP1, MYCN, GATA2, CDX2, FLI1, ZEB1, and HDAC2. The targets mentioned above control cellular activities such as proliferation, chromatin modification, cellular differentiation, the epithelial to mesenchymal transition, and apoptosis. Uncontrolled function of the mentioned transcriptional targets causes the cells to become transcriptionally plastic. SP1 is a cell cycle and apoptosis-related gene. MYCN regulates proliferative and metabolic pathways. GATA2 and CDX2 play a role in the pathway of differentiation and identity. FLI1 mediates the regulation of transcription and angiogenesis. ZEB1 is a master EMT controller. It exerts control via the repression of E-cadherin and the activation of the mesenchymal gene. HDAC2 exerts its silencing function via chromatin condensation. It mediates the silencing of the tumor suppressor gene (Cho et al., 2009; Wang et al., 2021).

Concomitantly, signaling factors such as PKA, PKR (EIF2AK2), PLCB1, and CJUN have been shown to be very important in stress response, inflammatory responses, calcium signaling, and protecting from apoptosis. CJUN is an AP-1 transcription factor that regulates growth and inflammatory responses. PKR helps in responses to cellular stress. PKA is involved in cAMP-mediated signals of protection from death, while PLCB1 regulates calcium-mediated signals. These signaling pathways help the TNBC cells to survive in conditions of hypoxia, oxidative stress, lack of nutrients, and chemotherapeutic drugs. (Figure 2.2)

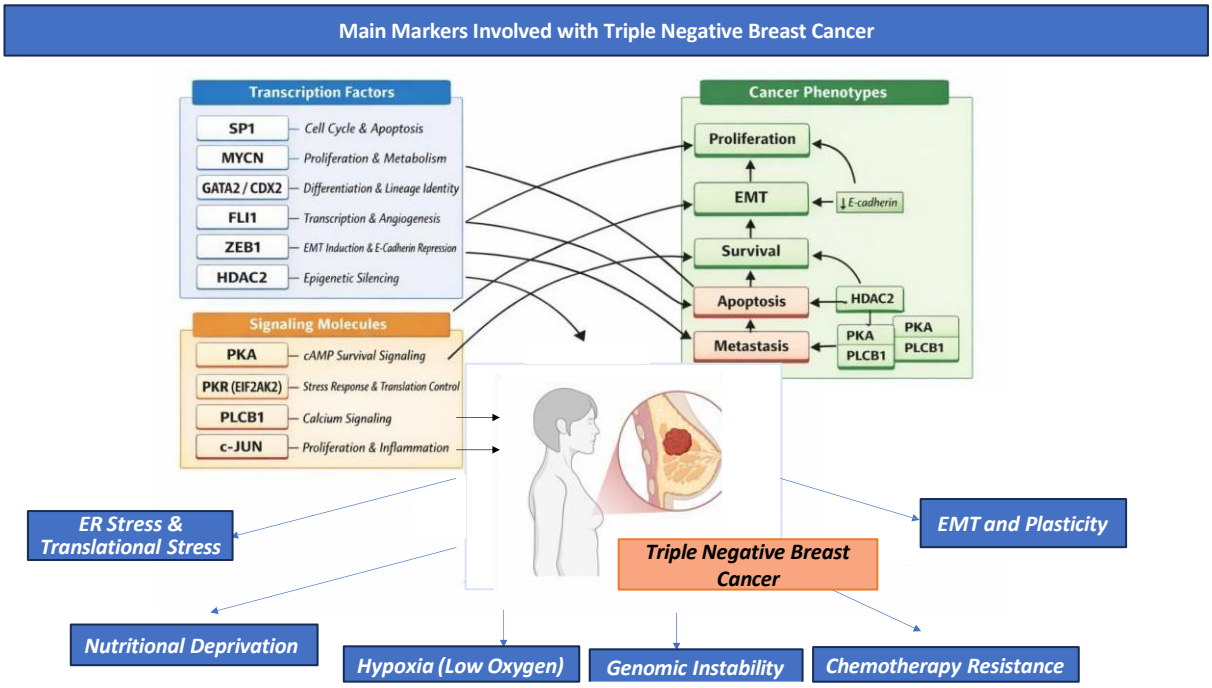

Figure 2.2: *Some of the major markers involved with Triple Negative Breast Cancer*

Beyond transcriptional and signaling dysregulation, TNBC cells are metabolically reprogrammed: they exhibit enhanced aerobic glycolysis, altered amino acid metabolism, increased glutamine dependency, redox imbalance, and mitochondrial dysfunction. These metabolic transformations provide energy, biosynthetic intermediates, and redox buffering capacity necessary for rapid proliferation and survival. Metabolic plasticity further supports EMT progression, immune evasion, and therapy resistance. Ultimately, TNBC is a complex disease driven by integrated transcriptional, signaling, apoptotic, adhesive, and metabolic networks rather than isolated oncogenic pathways (Guertin & Wellen, 2023; Sun et al., 2023).

Given the complexity, targeting a single pathway has resulted in limited clinical success. There is an emerging consensus that TNBC needs multi-target regulatory strategies capable of modulating several cancer hallmarks simultaneously. In the midst of such molecular complexity, metastasis suppressor genes have been identified as putative regulatory targets owing to their capacity to modulate multiple aspects of tumorigenesis. Among the identified genes is the *KISS1* gene, which encodes the kisspeptin protein, a peptide hormone. KISS1 initially introduced as a metastasis suppressor gene because of melanoma cells suppressed metastatic dissemination, without altering the development of the primary tumor, while being specifically expressed. However, kisspeptin is known for its importance in reproductive endocrinology owing to its receptor, KISS1R/GPR54, involvement in the regulation of the gonadotropin release.(de Roux et al., 2003)

Apart from reproductive biology, kisspeptin has recently emerged as a regulatory factor for cancer progression. Kisspeptin expression has been shown to inhibit migration, invasion, EMT, angiogenesis, and metastasis in various cancer types such as melanoma, ovarian cancer, pancreatic cancer, colorectal cancer, and gastric cancer. Such findings have established kisspeptin as a candidate tumor suppressor (Cvetković et al., 2013a)

Kisspeptin has been shown to modulate several transcription factors involved in differentiation and EMT. It inhibits the mesenchymal transcript profile and induces an epithelial phenotype. At the adhesive surface, it has been demonstrated that kisspeptin induces the expression of epithelial cell surface proteins like E-Cadherin (*CDH1*) and Beta-Catenin (*CTNNB1*), which play crucial roles in maintaining cell-cell junctions and epithelial polarity. Expression of these proteins improves intercellular adherence but abrogates migration.(Iseki et al., 2017). Concomitantly, kisspeptin also reduces mesenchymal and stemness-related markers such as N-Cadherin (*CDH2*), vimentin (*VIM*), and CD44, characteristic of EMT, invasion, and cancer stem cell-like properties. Downregulation of CD44 is especially important as it is linked to tumor formation, chemo-resistance, and the colonization of metastasis. Thus, by regulating such a complex array of markers, Kisspeptin also brings about a mesenchymal to epithelial transition (MET), thereby suppressing the potential.

In parallel, Kisspeptin strongly influences apoptotic machinery. It modulates key apoptotic regulators such as BAX, BCL2, CASPASE-3, CASPASE-8, and CASPASE-9, indicating activation of both intrinsic and extrinsic apoptotic pathways. BAX promotes mitochondrial membrane permeabilization, leading to cytochrome c release and activation of CASPASE-9. CASPASE-9, in turn, activates CASPASE-3, the executioner caspase responsible for DNA fragmentation and cellular dismantling. CASPASE-8 represents the extrinsic pathway of apoptosis initiated by death receptor signaling. Concurrent suppression of BCL2 removes anti-apoptotic protection and tips the balance toward programmed cell death (Carneiro & El-Deiry, 2020; Mustafa et al., 2024).

This coordinated regulation of apoptosis thus ensures that not only is the migration of TNBC cells prevented, but these are driven toward an irreversible commitment to apoptosis. Such dual control over migration and survival is of special value in combating metastatic cancer. The peptide also modulates intracellular signaling pathways like MAPK, PI3K/AKT, and cAMP/PKA, which control cellular proliferation, survival, metabolic processes, and response to stress. With the modification of these signaling cascades, kisspeptin exerts pleiotropic regulatory effects more than isolated molecular targets.

Recent metabolomics data also supports that kisspeptin has a regulatory function in redox homeostasis, amino acid metabolism, purine metabolism, lipid metabolism, and cytotoxic metabolism pathways. Glutathione metabolism is a marker of redox imbalance; changes in amino and purine metabolisms are indicative of biosynthesis and energy metabolism pathways. The presence of cytotoxic and anti-angiogenic metabolites after kisspeptin treatment points towards metabolic pathways in support of apoptosis and anti-proliferative pathways. Kisspeptin thus acts as a systemic modulator of cell fate regulation by coordinating transcriptional, signaling, adhesive, apoptotic, and metabolic pathways (Lee et al., 2018).

Considering such encouraging findings, there have been very few comprehensive studies encompassing the role of kisspeptin regarding EMT, apoptosis, metabolism, as well as the regulation of genes via kisspeptin in TNBC. Indeed, almost all prior studies have been conducted on an individual molecular basis, which has failed to identify the broader gene expression profile. In fact, there has been insufficient investigation regarding the prognosis-based gene expression of genes influenced by kisspeptin, as well as the markers of apoptosis/adhesion for TNBC patients, alongside the TNBC subtype-based efficacy of kisspeptin treatment.

Therefore, the current study was specifically designed to understand the molecular and functional impact of exogenous Kisspeptin-10 in triple-negative breast cancer. Using combined in vitro, in silico, transcriptomic, and metabolomic approaches, this study aims to define how kisspeptin controls transcription factors, signaling molecules, EMT and adhesion markers, apoptotic regulators, and metabolic pathways in TNBC. The study will also validate the clinical relevance of these molecular changes using publicly available patient datasets. By this multidimensional approach, the present work attempts to establish the role of kisspeptin as a pleiotropic regulator capable of reprogramming TNBC cells toward a less aggressive, less migratory, and more apoptosis-prone phenotype. Elucidation of this regulatory network may provide novel insights into the therapeutic potential of kisspeptin in the management of triple-negative breast cancer and may contribute to the development of future multi-target therapeutic strategies for this aggressive disease.

HYPOTHESIS

Does exogenous Kisspeptin-10 restore normal KISS1 signaling in triple negative breast cancer (TNBC) cells, which in turn alters the expression of key genes, inhibits EMT and metastasis, re-establishes adhesion molecules, initiates apoptosis, and reprograms metabolism to render TNBC cells less aggressive and more apoptotic?

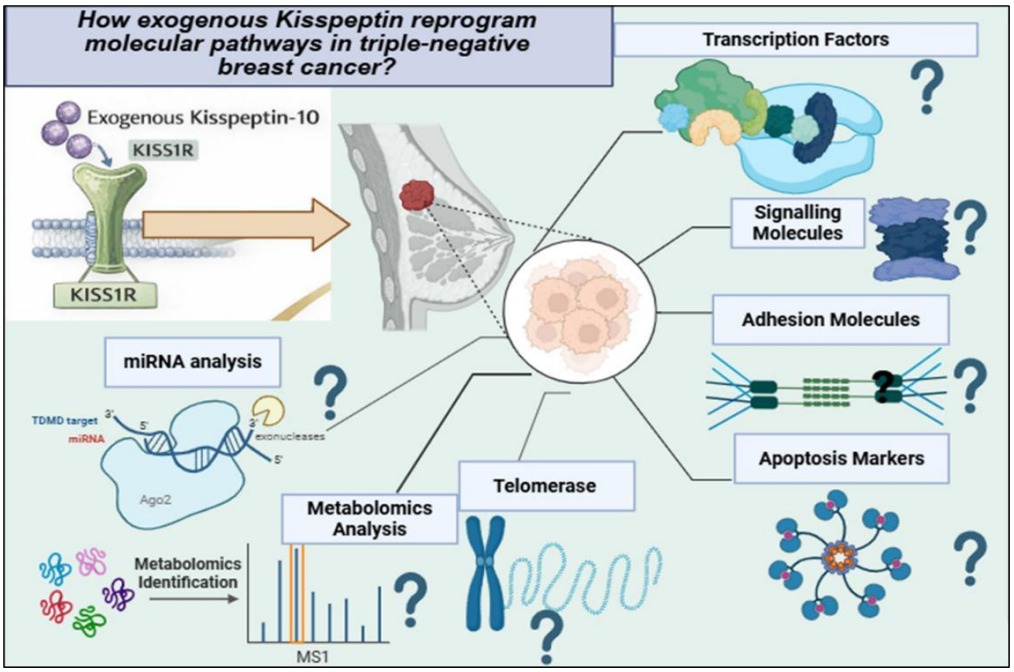

Figure 2.3: *Hypothesis on how Kisspeptin reprograms molecular pathway in Triple Negative Breast Cancer.*

2.3.1 Cell Culture Maintenance

As an experimental model, MDA-MB-231 and MDA-MB-468 cells, a human TNBC cell line, were acquired from the National Centre for Cell Sciences (NCCS), Pune. In order to give necessary growth, cells were cultivated in Leibovitz's L-15 media (HiMedia, AL011A) supplemented with 10% foetal bovine serum (FBS; Gibco; 26140079) and 1% penicillin-streptomycin. Under atmospheric circumstances, the cells were kept at 37°C. After purchasing Kisspeptin-10 (YNWNSFGLRF-NH2) (M2816) from Sigma Aldrich, an exogenous therapy regimen was implemented.

2.3.2 Overall Experimental Regime

To investigate the molecular effects of Kisspeptin-10 in TNBC, the current study used an integrated in vitro-in silico experimental framework. MDA-MB-231 cells seeded in 96-well multi-well plates (5000–10,000 cells/well) were exposed to several concentrations of Kisspeptin-10 (10, 25, 50, 100, 200, 500, and 1000 nM) for a duration of 24 hours. The MTT test was used to measure cell proliferation (HiMedia: TC191). Kisspeptin-10 was administered to MDA-MB-231 and MDA-MB-468 cells at the determined inhibitory concentrations of 10 (IC10) and 50 (IC50) based on the MTT assay. Untreated and doxorubicin-treated cells were used as negative and positive controls, respectively. To ensure consistency in the results, each experiment is independently conducted at least three times using suitable technical and biological replicates. The following doses were administered: Kisspeptin-10-IC_{10}: 12.13 nM, Kisspeptin-10-IC_{50}: 110.21 nM Doxorubicin-HCL-IC_{10}: 62.38 nM, Doxorubicin-HCL-IC_{50}: 442.30 nM (Figure 2.4).

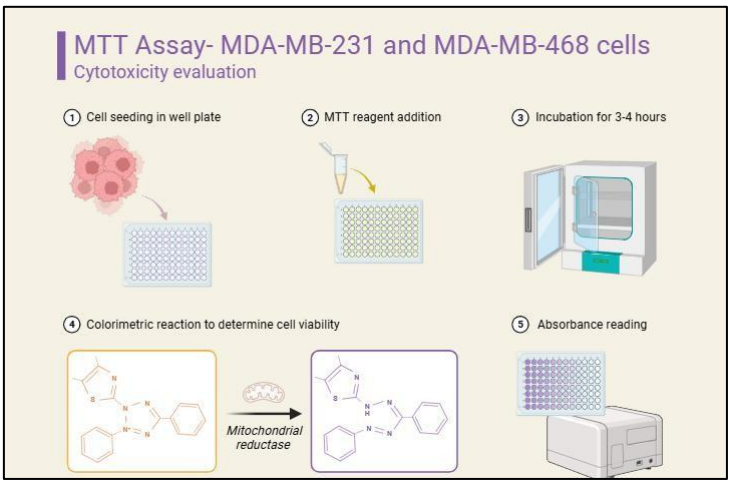

Figure 2.4: Cell Cytotoxicity Assay for both the cell lines

Hence, there are five groups:

1. Control: Untreated Cells
2. Kisspeptin-10-IC_{10}: 12.13 nM (K10) for MDA-MB-231 and 9.31 nM (K10) for MDA-MB-468
3. Kisspeptin-10- IC_{50}: 110.21 nM (K50) for MDA-MB-231 and 88.35 nM (K50) for MDA-MB-468
4. Doxorubicin-HCL-IC_{10} (positive control): 62.38 nM(D10) for MDA-MB-231 and 39.24 (D10) for MDA-MB-468
5. Doxorubicin-HCL- IC_{50} (positive control): 442.30 nM(D50) for MDA-MB-231 and 378.35(D50) for MDA-MB-468

2.3.3 Cell Migration Assay

The migratory capacity of MDA-MB-231 and MDA-MB-486 cells in response to kisspeptin administration was assessed using the wound-healing test. After growing the cells to 80% confluence, they were plated on 6-well plates at a density of 2×10^5 cells/well. A 200 µL tip was used to create a uniform wound. Following a 24-48-hour treatment with and without kisspeptin, the cells were resuspended in PBS. The inverted phase-contrast microscope was used to take pictures of the wound at 0, 12, and 24 hours. ImageJ software was then used to analyse the migratory distance. (Figure. 2.5)

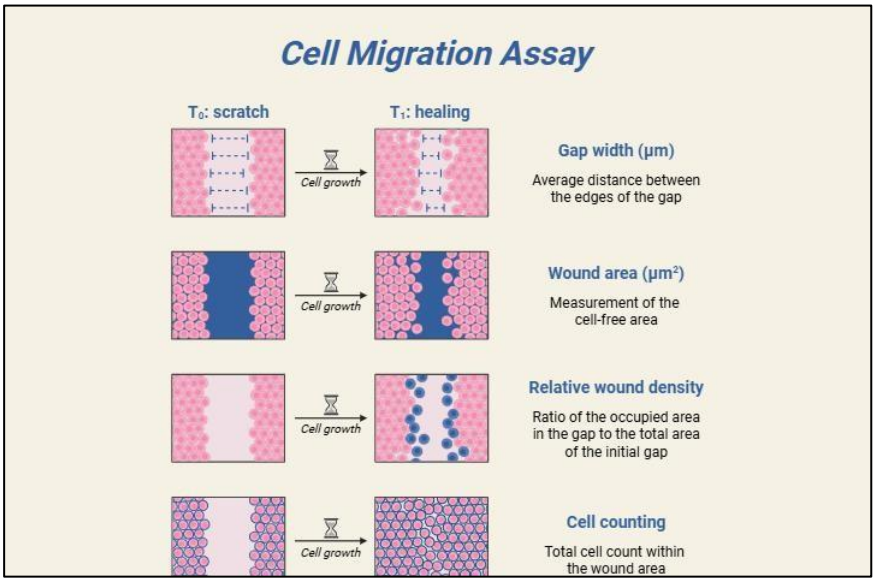

Figure 2.5a: *Cell Migration Assay for both the cell lines*

2.3.4. Cell Invasion Assay

MDA-MB-231 and MDA-MB-468 cells's invasive capability was assessed using a Matrigel-coated trans-well test with 8µm pore inserts. Chambers were pre-coated with Matrigel to mimic the extracellular matrix. Cells (1×10^5) were seeded in serum-free media in the upper chamber, while chemoattractant medium with 10% FBS was added to the lower chamber. Kisspeptin at concentrations of (K10) and (K50) was used to treat cells for 24 hours. The non-invading cells were removed from the upper side of the membrane, and the cells that migrated to the lower surface were fixed, stained with Giemsa, and counted under a light microscope.

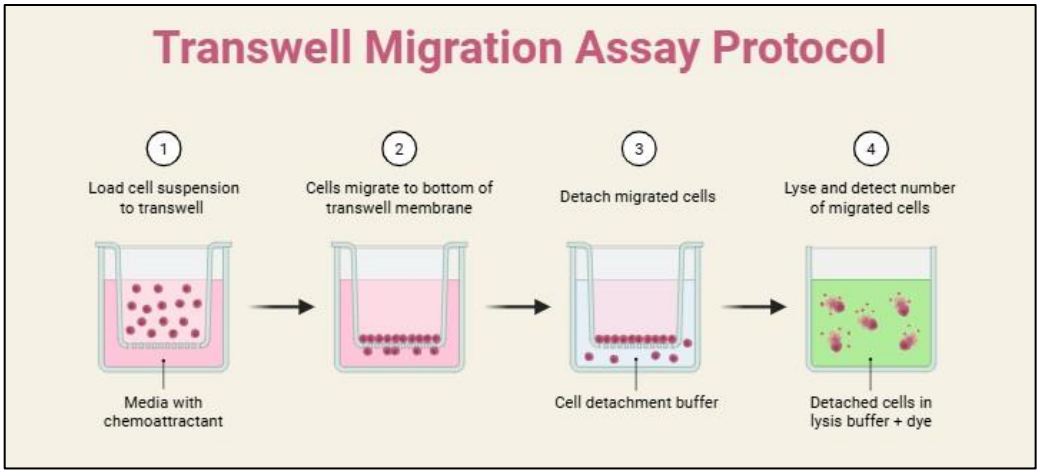

Figure 2.5b: *Cell Invasion Assay for both the cell lines*

2.3.5 RNA Isolation, cDNA synthesis, and qRT-PCR

Total TRIzol™ reagent was used in accordance with the protocol to extract RNA from cells. Cells were scrapped in 1 mL of TRIzol without the presence of RNase. Chloroform was added after incubation, and phase separation was then achieved by centrifugation. After carefully transferring the RNA-containing aqueous phase, the RNA was precipitated using isopropanol, rinsed with 75% and 100% ethanol in succession, allowed to air dry, and then dissolved in nuclease-free water treated with DEPC. A Shimadzu BioSpec-nano NanoDrop spectrophotometer was used to measure the concentration and purity of RNA. A260/A280 ratios ranging from 1.8 to 2.0 were deemed appropriate for the samples.

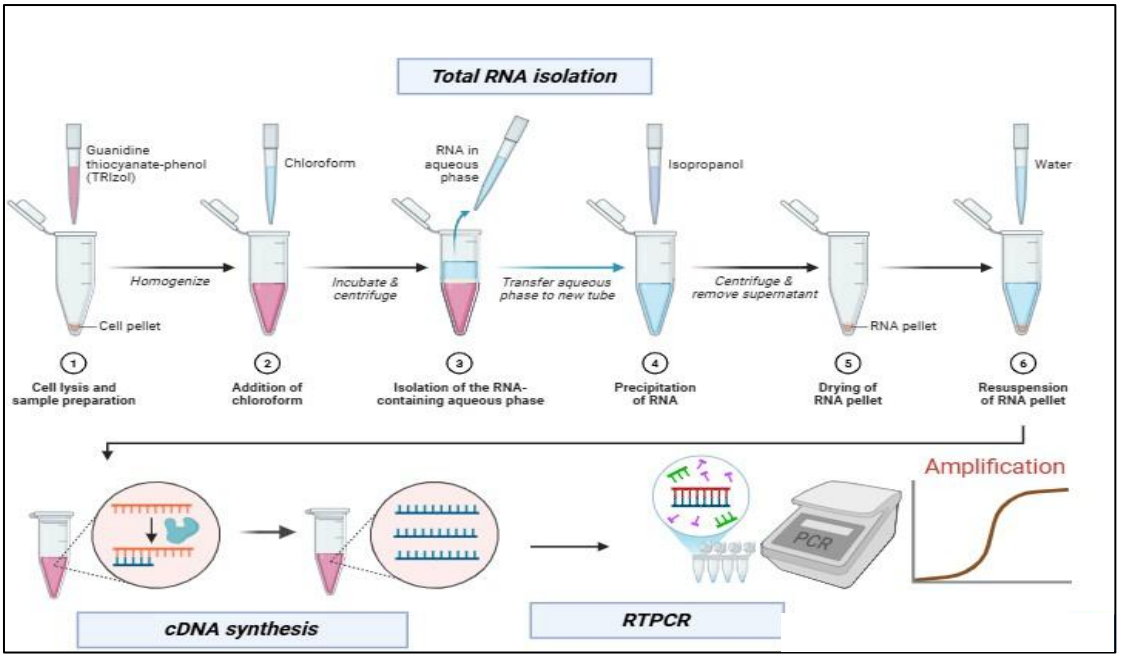

Figure 2.6a: RT-PCR workflow

cDNA Synthesis

Complementary DNA (cDNA) was synthesized from 1 µg of total RNA using the High-Capacity cDNA Reverse Transcription Kit (Thermo Fisher Scientific, Cat. No. 4368814) following the manufacturer's protocol.

Table 2.1 Composition of cDNA synthesis master mix (per reaction)

Component	Volume (µL)
10X RT Buffer	2.0
25X dNTP Mix (100 mM)	0.8
10X RT Random Primers	2.0
Reverse Transcriptase	1.0
Nuclease-Free Water	4.2
Total	**10.0**

Each reaction contained 10 µL RNA sample and 10 µL master mix, giving a final volume of 20 µL.

Table 2.2 Thermal Cycler Conditions for cDNA Synthesis

Step	Temperature	Time
Primer annealing	25°C	10 min
cDNA synthesis	37°C	120 min
Enzyme inactivation	85°C	5 min
Hold	4°C	∞

Synthesized cDNA was stored at −20°C until further use.

Primer Design

Primers were designed for SP1, CDX2, GATA2, C-MYC, FLI1, ZEB1, PRKACA (PKA), EIF2AK2 (PKR), PLCB1, CJUN, E-cadherin, N-cadherin, Vimentin, β-catenin, CD44, BCL2, BAX, CASPASE-3, CASPASE-8, CASPASE-9, and HTERT using NCBI Primer-BLAST. Primer properties were validated using OligoCalc. Primer sequences are listed in **Table 2.3.**

- Design criteria included:
- Primer length ~20 bp
- Tm between 57–59°C
- GC content 50–55%
- Amplicon length 50–150 bp
- Absence of hairpins, dimers, and repeatsAll primers were synthesized commercially, reconstituted to 100 µM stock, and diluted to 10 µM working concentration. The amplification curve can be found in Appendix 1.

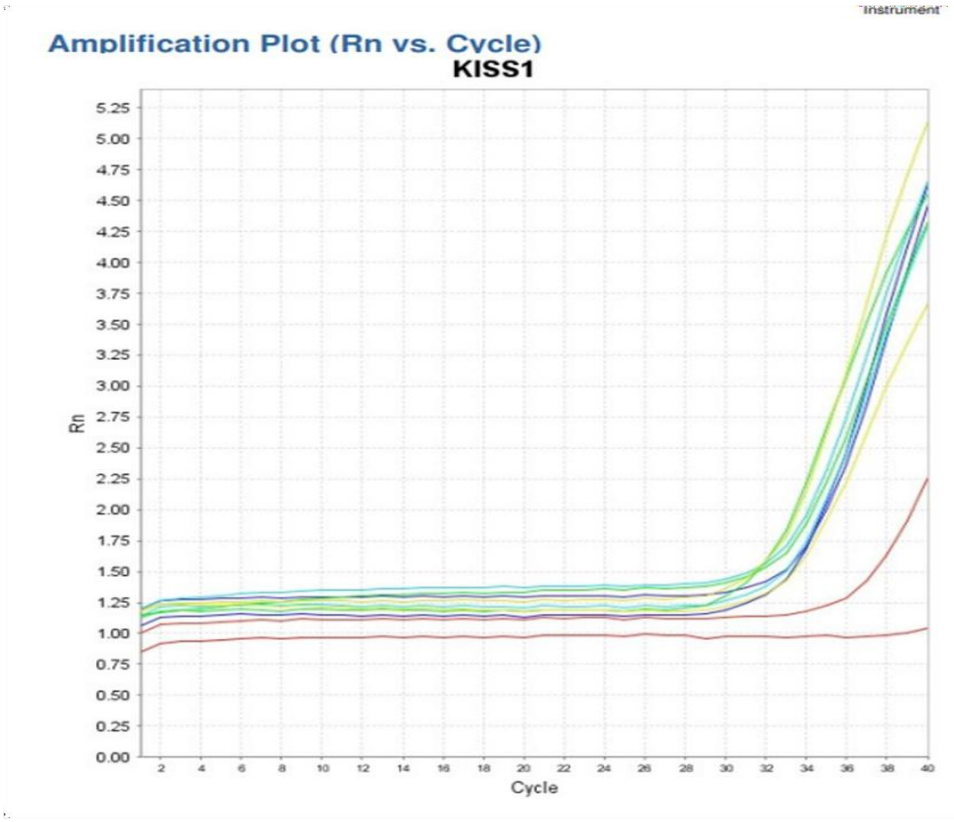

Figure 2.6b: *Representative amplification curve for KISS1 for gene expression analysis*

Table 2.3: List of Primers designed for qRT-PCR.

Gene	Forward Primer (5′→3′)	Reverse Primer (5′→3′)	NCBI RefSeq (mRNA)	PCR Product Size
SP1	GGCCTCCAGACCATTAACCT	GAAGGTGATTGTTTGCCTGG	NM_138473.4	255 bp
NMYC	CACAAGGCCCTCAGTACCTC	GAGGTTTGGGTAGTGTGTCC	NM_005378.6	188 bp
GATA2	GTGACCTGTTGAGGCACTTG	TTCTGCTGTGACCCAGTCTC	NM_001145661.2	228 bp
CDX2	GGAAGTGAGCGACGGTGACT	TGTAGGCAGTGTAGGCGTGA	NM_001265.5	185 bp
HDAC2	TTCTGCTGACAGTGCCTTTC	AGTGGCTTGGAACGAGTTTG	NM_001527.4	195 bp
FLI1	GCAGAGCGACAACCTGAGT	GTCATGTTGAGCGGTTGTTG	NM_002017.5	229 bp
ZEB1	CTGGTGTTGATGATGCCAGT	GCTGTTGCTTTCCTTTCCTG	NM_030751.6	225 bp
ECAD (CDH1)	TGCCCAGAAAATGAAAAAGG	GTGTATGTGGCAATGCGTTC	NM_004360.5	195 bp
NCAD (CDH2)	AACTGTGACCGATAAGGATC	GATCCTGTGAATGGACAAAT	NM_001308176.2	205 bp
VIMENTIN	GAGAACTTTGCCGTTGAAGC	GCTTCCTGTAGGTGGCAATC	NM_003380.5	204 bp
BCATENIN	TATTGTACGTACCATGCAGA	GGAATGCAAGCTTTAGGACTT	NM_001330729.2	212 bp
CD44	GAGCATCGGATTTGATGATGAC	CATTGTGGGCAAGGTGCTATT	NM_001202555.1	222 bp
PKA (PRKACA)	CCCGTGATGACCTGCTTGAA	GTTGCGATGGCTTCAGGTAG	NM_002730.4	191 bp
EIF2K2 (PKR)	GGCAAAACTTGATCATGTA	TACATGAGCCCAGAACAGAT	NM_002759.4	221 bp

PLCB1	CCACTGGAATCTGGAGTTCC	AGAAGAAATGTCTAATCTGG	NM_182734.3	255 bp
CJUN	CATCGACATGGAGTCCCAGG	GACAAGTTGCGACGGAGAGA	NM_002228.4	228 bp
BCL2	ATGTGTGTGGAGAGCGTCAA	GGAGGAGAAGATGCCGGTTC	NM_000633.3	230 bp
BAX	TTTGCTTCAGGGTTTCATCC	GACACTCGCTCAGCTTCTTG	NM_138761.4	214 bp
CASPASE 3	AGAACTGGACTGTGGCATTGAG	GCTTGTCGGCATACTGTTTCAG	NM_004346.4	198 bp
CASPASE 8	GGTCACTTGAACCTTGGGAA	AGGCCAGATCTTCACTGTCC	NM_001354782.2	224 bp
CASPASE 9	AGATGTCGGCCTTTGTGTTT	GTTTCGTAGGCTGCTGTCGA	NM_001229.5	196 bp
KISS1	TGCTGCTTCTCCTCTGTGTG	AGGCTTGCTCTCTGCATACC	NM_002256.3	~150 bp
KISS1R	TGTCAGCCTCAGCATCTGGGTA	CAGCAGGTTGTACAGTGCGAAG	NM_032551.5	~110 bp
hTERT	CGTACAGGTTTCACGCATGTG	ATGACGCGCAGGAAAAATG	NM_198253.2	~150 bp

Quantitative Real-Time PCR (qRT-PCR)

qRT-PCR was performed using SYBR Green Master Mix (Thermo Fisher Scientific, Cat. No. A25742). β-actin served as the endogenous control gene. All reactions were performed in triplicate along with no-template controls.

Table 2.4: Reaction Setup for qPCR (10 µL)

Component	Volume (µL)
SYBR Green Master Mix	5.0
Forward Primer (10 µM)	0.5
Reverse Primer (10 µM)	0.5
Nuclease-free Water	3.0
cDNA Template	1.0
Total	10.0

Table 2.5: Thermal Cycler Profile

Step	Temperature	Duration	Cycles
UDG Activation	50°C	2 min	Hold
Initial Denaturation	95°C	2 min	Hold
Denaturation	95°C	15 sec	40
Annealing	57–60°C	15 sec	
Extension	72°C	1 min	

Melting curve analysis was performed to confirm amplification specificity.

2.3.6 miRNA isolation and quantitative real-time PCR (qPCR)

Total RNA, including small RNAs, was obtained using the miPremier microRNA Isolation Kit (Merck) (SNC50). The quality was checked using agarose gel, and the amount and purity were analyzed using NanoDrop spectrophotometry (260/280 ratio of 1.8-2.0). miRNA cDNA synthesis: This was done using the TaqMan™ Advanced miRNA cDNA Synthesis Kit (Applied Biosystems). This process involves poly(A) tailing, adapter ligating, and universal reverse transcription. Primer for additional miRNA expression for miRNA-200, miRNA-345, and miRNA-577 are as indicated below (Table 2.6) for additional miRNA expression. U6 snRNA was employed as the endogenous reference gene for normalization. Standards for qPCR analysis as recommended by the MIQE guideline were maintained for both the primer and standards for amplification efficiency (range 90-110 %).

Table 2.6: Primer for additional miRNA expression

miRNA Name		Sequence
hsa-miR-200c-3p	miRB	CGUCUUACCCAGCAGUGUUUGG
hsa-miR-345-3p	miRB	GCCCUGAACGAGGGGUCUGGAG
Has-miR-577	miRB	UAGAUAAAAUAUUGGUACCUG

2.3.7 Western Blot Analysis

Protein Estimation by Bradford Assay

MDA-MB-231 and MDA-MB-466 control vs the treated cells were quickly washed with sterile 1× phosphate buffered saline (PBS, pH 7.4) to remove residual debris. On ice, the cells were scraped were taken in ice-cold RIPA lysis buffer composition of 150 mM NaCl, 1% NP-40, 0.5% sodium deoxycholate, 0.1% SDS, and 50 mM Tris-HCl, pH 8.0 to which freshly added protease inhibitor cocktail was supplemented. Cells were centrifuged at 12,000 rpm for 15 minutes at 4°C, followed by

collecting the supernatants containing total protein extracts and storing them at −80°C until further analysis.

The protein concentration was estimated by Bradford protein assay reagent (SRL, Cat. No. 19219). The Bradford protein assay reagent was diluted at a ratio of 1:5 with distilled water, and this reagent mixture was used for protein concentration calculation. A stock of BSA standards ranged from0–750 µg/mL µg/mL to construct a calibration curve for protein concentration calculations. The protein sample was diluted at a ratio of 1:5 with distilled water, and 10 µL of protein sample was aliquoted onto a 96-well plate and incubated with 200 µL protein assay reagent for a period of 10–30 minutes in the dark at room temperature. The protein concentration was estimated by a plate reader at a wavelength of 595 nm.

All samples were normalized to equal protein concentrations and treated by mixing each sample with 2X Laemmli Sample Buffer and 10% β-Mercaptoethanol. The samples were boiled at 100°C for 6-7 minutes, then stored in a frozen state at -20°C until the electrophoresis procedure was started. About 40 µg of protein per sample was resolved in 10% SDS-PAGE gels in the presence of a buffer containing 25 mM Tris, 190 mM glycine, a percentage of SDS equal to 0.1%, and a pH of 8.3 for a total of 80 V until the sample was fully separated. The separated protein was transferred to a PVDF membrane previously treated for 2-3 minutes with methanol in a wet transfer buffer containing the aforementioned buffer components but for a percentage of 20% methanol for a total of 80 V for a total of 1hr30 min at a temperature of +4°C.

Post transfer, the membranes were quickly stained with Ponceau solution to verify the reliability of protein transfer and integrity. The membranes were destained with both water and TBST solution. The membranes were then blocked in 3–5% skim milk solution in TBST for 1 hour at room temperature, avoiding nonspecific binding. The membranes were then probed overnight with the primary antibodies in 3% skim milk solution, agitating the membranes with a gentle motion at 4°C. After incubating membranes with primary antibody, they were washed three times in TBST buffer for 7 minutes each and incubated using appropriate HRP-conjugated secondary antibodies for a period of 1.5 hours at room temperature under gentle shaking conditions. After incubating membranes using secondary antibodies, they were washed three times in TBST buffer for 5 minutes each.

The protein bands were visualized using a diaminobenzidine (DAB) chromogenic detection method. The DAB substrate was applied uniformly to cover all areas until bands were visible. This was terminated by washing in water and photographing after air-drying for densitometric analysis using ImageJ software.

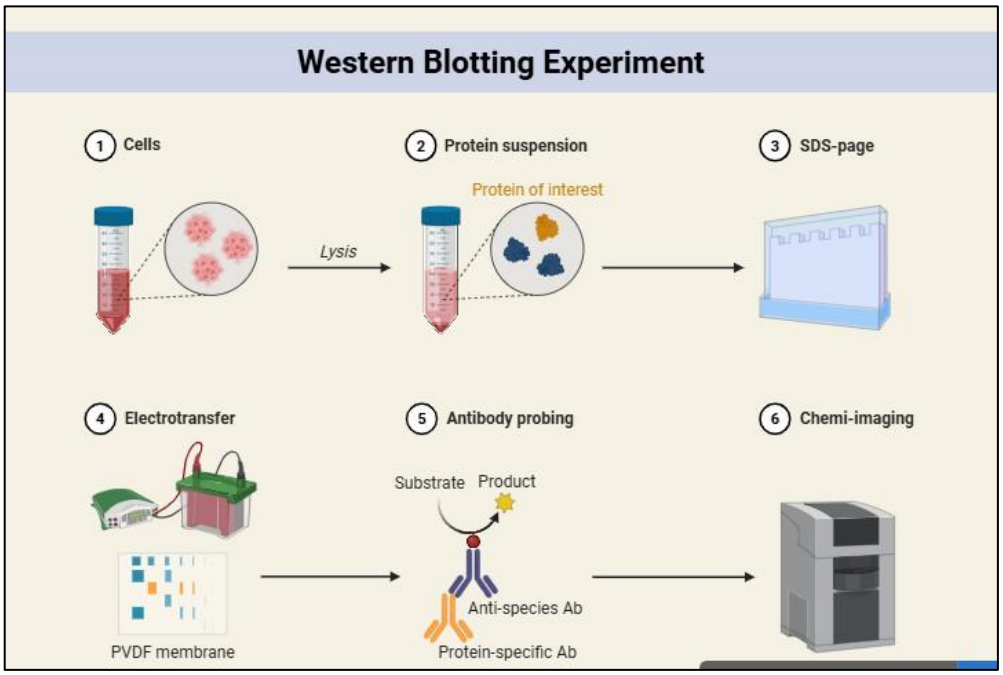

Figure 2.7: Western Blot Experiment Workflow

Table 2.7 (a) : Bradford Assay Standard Curve Preparation

BSA Volume (µL)	Concentration (µg/mL)	PBS Volume (µL)	Bradford Reagent (µL)
7.5	750	12.5	200
5.0	500	15.0	200
2.5	250	17.5	200
1.5	150	18.5	200
1.0	100	19.0	200
Blank	0	20.0	200

Table 2.7 (b) : Bradford Assay Results for Experimental Samples

Sample	OD 1	OD 2	Mean OD	Protein Concentration (mg/mL)	Working Volume for 40 µg (µL)
Control	1.523	1.453	1.5207	0.7566	132.18
K10	1.563	1.594	1.5570	0.7746	129.09
K50	1.504	1.504	1.5280	0.7602	131.54
D10	1.500	1.483	1.4413	0.7171	139.45

D50	1.499	1.589	1.4960	0.7443	134.36

Based on these calculations, equal amounts of protein (40 µg) were standardized for all samples to ensure uniform loading during Western blotting.

Table 2.8: Sample Volume Calculation for 40 µg Protein Loading

Sample	Protein Concentration (mg/mL)	Volume for 40 µg (µL)
Control	0.7566	132.18
K10	0.7746	129.09
K50	0.7602	131.54
D10	0.7171	139.45
D50	0.7443	134.36

Table 2.9: Preparation of Samples for SDS-PAGE

Sample	Protein Volume (µL)	2X SDS Buffer (µL)	Final Volume (µL)
Control	132.18*	Equal volume	40
K10	129.09*	Equal volume	40
K50	131.54*	Equal volume	40
D10	139.45*	Equal volume	40
D50	134.36*	Equal volume	40

The Western blot technique employed the Bio-Rad Mini-Protean system. A 12% resolving gel and a 5% stacking gel were prepared. For all the samples of the Protein Quantification technique, the Western blot technique is employed. The materials and equipment required for the technique are as described below:

Table 2.10: Reagents used in Western Blot Experiment

Reagent	Volume	Composition
1.5 M Tris-HCl	1 L	Tris base: 181.5 g pH set to 8.8
0.5 M Tris-HCl	100 mL	Tris base: 6.05 g

		pH set to 6.8
10% SDS	10 mL	SDS: 1g
10% APS	1 mL	APS: 0.1 g
1% Bromophenol Blue	10mL	BPB: 0.1g
10X Running Buffer	500 mL	250 mM Tris-HCl: 15.15g 1.92 M Glycine: 72.05g 1% SDS: 5g
1X Running Buffer	500 mL	10X Running Buffer: 50 mL
10X Transfer Buffer	500mL	250mM Tris-HCl: 15.15g 1.92M Glycine: 72.05g
1X Transfer Buffer (20% methanol)	500mL	10X Transfer Buffer: 50 mL Methanol: 100 mL
10X TBS	500 mL	200 mM Tris base: 12.11 g 1.5 M NaCl: 44 g pH set to 7.6
1X TBS-T (1% Tween-20)	500 mL	10X TBS: 50 mL Tween-20: 5 mL
10X PBS	500 mL	1.37 M NaCl: 8.9 g 270 mM KCl: 1.2 g 100 mM Na2HPo4: 40 g 18 mM KH2PO4: 1 g
1X PBS	500 mL	10X PBS: 50 mL
5% Blocking buffer	50 mL	BSA: 2.5 g Solvent: 1X PBS

Table 2.12: Gel Composition for SDS-PAGE

Component	5% Stacking Gel (mL)	12% Resolving Gel (mL)
Distilled Water	3.4	3.3

Tris-HCl	0.625 (0.5 M, pH 6.8)	2.5 (1.5 M, pH 8.8)
30% Acrylamide	0.05	4.0
10% SDS	0.05	0.10
10% APS	0.05	0.10
TEMED	0.006	0.006

Table 2.13: Target Antibodies with the catalogue number

Target Protein	Company	Catalogue Number	Dilution
ZEB1	Abclonal	A5600	1:1000–1:1500
SP1	Abclonal	A14662	1:1000–1:1500
GATA2	Abclonal	A0677	1:1000–1:1500
CDX2	Abclonal	A1629	1:1000–1:1500
PKA (Catalytic subunit)	Thermo Fisher	PA5-17626	1:1000
PLCB1	Thermo Fisher	PA5-96018	1:1000
c-Jun	Thermo Fisher	PA5-88120	1:1000
Kisspeptin (KISS1)	Thermo Fisher	PA5-106920	1:1000
FLI1	Thermo Fisher	PA5-29597	1:1000
KISS1R	Bioss	bs-2501R	1:5000
Anti-rabbit HRP Secondary	Thermo Fisher	G-21234	1:1000
β-Actin	Santa Cruz	Sc-47778	1:500
ECAD	Santa Cruz	Sc-8426	1:1500

2.3.8 Metabolomic Profiling:

For Control and Kisspeptin-treated MDA-MB-231 cells, untargeted metabolomics analysis was conducted to understand the trend of alteration of metabolites. Cold MeOH/water solution of 80:20 v/v was used as a solvent to extract the metabolite of interest. It was then vortexed, followed by centrifugation at 14,000 rpm for 10 minutes at 4°C. Both positive- and negative electrospray ionization modes of LC-MS were used to study the supernatant of the cell culture. MS converter was used to identify the metabolite of interest, generating a qualitative volcano plot. Pathway enrichment analysis of the metabolite network pathway was done via Cytoscape. Altered pathways were also determined via visualization of a metabolite network pathway.

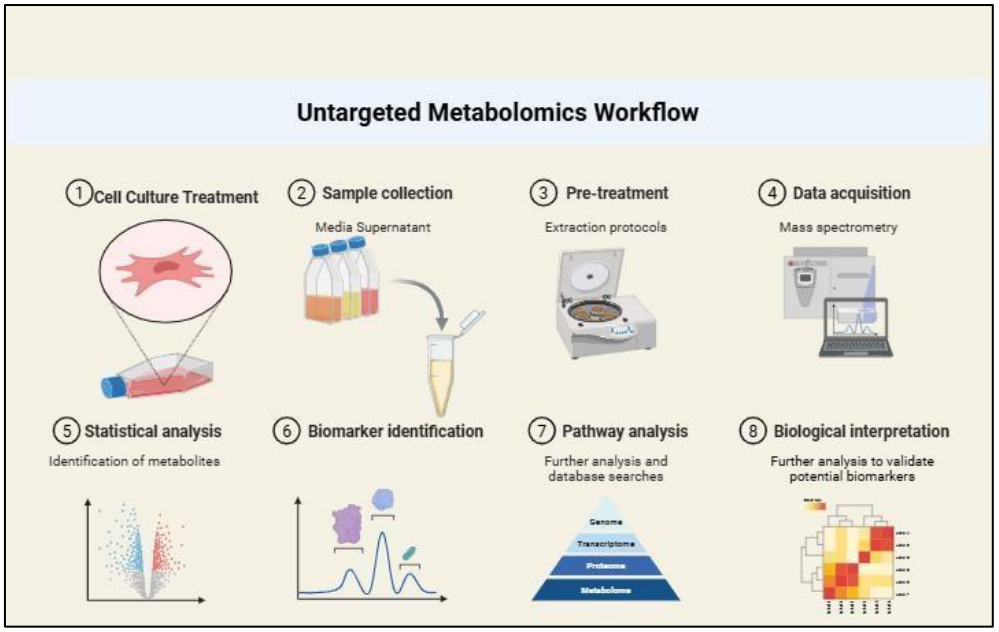

Figure 2.8: *Metabolomics Workflow*

2.3.9 In silico Expression and Prognostic Analysis

Publicly available transcriptomic datasets were used to confirm experimental results and to explore clinical relevance of significant genes. UALCAN, http://ualcan.path.uab.edu, was used to analyze differential gene expression between TNBC and normal tissues by using TCGA data. For visualization of the tumor-vs-normal expression differences, KISS1. Kaplan–Meier survival plots were constructed with KM Plotter, http://kmplot.com, to assess the correlation of gene expression with OS of breast cancer patients for following genes: SP1, C-MYC, HDAC2, ZEB1, CDX2, GATA2, and FLI1, PRKACA (PKA), EIF2AK2 (PKR), PLCB1, and CJUN, Ecadherin, N-cadherin, Vimentin, β-catenin, CD44, BCL2, BAX, CASPASE 3, CASPASE 8, and CASPASE 9.

Computational Transcriptomics Analysis of Public Gene Expression Datasets in TNBC and Non-TNBC Samples:

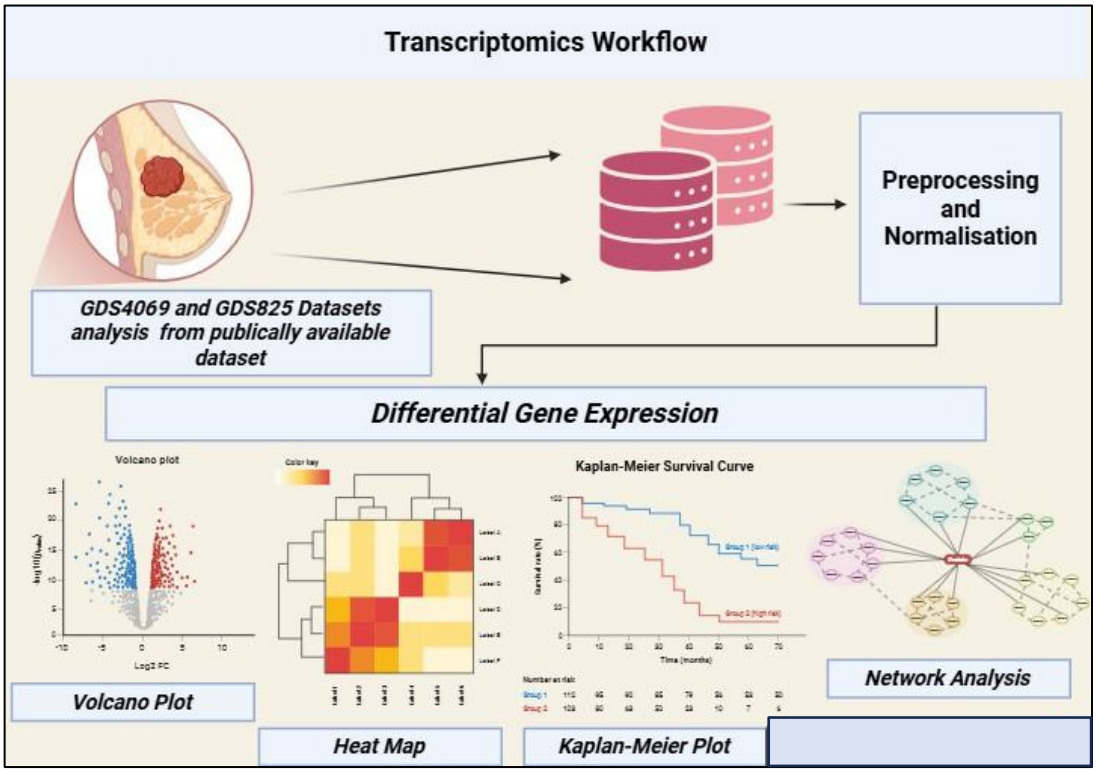

Figure 2.9: Transcriptomics Workflow

Two publicly available transcriptomic datasets, GDS4069 and GDS825, were downloaded from the NCBI Gene Expression Omnibus (GEO) database to explore specifically differentially expressed genes associated with TNBC. Samples included in both datasets are well-annotated TNBC and non-TNBC breast cancers. The raw CEL files of datasets were preprocessed and then normalized using the affy and limma packages in R. Expression matrices that have been normalized were downloaded directly and log2 transformed. Gene annotation was performed using the corresponding GEO platform files. Those genes for which there were more than one probe were reduced to one probe with a maximum average expression across all samples. Empirically, the genes having low expression across all samples were filtered out. Then, differential gene expression analysis was performed to identify transcriptional changes distinguishing TNBC from other non-TNBC subtypes within each dataset. Microarray data were analyzed using the limma package, while RNA-seq data were analyzed using the DESeq2 package.

Next, volcano plots have been used to visualize the genome-wide expression changes in terms of fold change value along with significance in expression changes for each DEG in TNBC samples compared to non-TNBC samples. To carry out the analysis in a non-biased fashion, only those DEGs that are commonly observed in GDS4069 as well as GDS825 datasets are selected for further analysis, resulting in the consensus DEG dataset consisting of approximately 70 genes which are further analyzed using hierarchical clustering, performed using the z-score method, which on further application, resulted in

the visualization of the clustered results via the heatmap function in R, provided via the package 'pheatmap.' To analyze the regulatory impact, a list consisting of approximately 20 transcription factors, regulators, etc., i.e., SP1, ZEB1, TCF12, CASP3, PKA, etc., which are known regulators in transcription regulation, metastasis, apoptosis, chromatin remodeling, are curated from the database TFLINK, which are then used to create a bipartite network consisting of these regulators with the common DEGs, where the existing relationship involving DEGs with these regulators in the bipartite network is taken care of with the Cytoscape version 3.10.0 package.

2.3.10 Data Analysis

All statistics were done using GraphPad Prism software, version 8.0. Data from experiments are expressed as the mean ± SEM, unless otherwise indicated. Where appropriate, data were tested for normality and homogeneity of variance before hypothesis testing; these tests confirmed that the assumptions necessary for a parametric analysis were met.

Comparisons among more than two experimental groups were made by one-way ANOVA. When ANOVA indicated that the overall difference was statistically significant, Duncan's New Multiple Range post hoc test was conducted to find the specific differences among groups. To assess the results, it was assumed that the results would be statistically significant at $*p < 0.05$, $**p < 0.01$, or $***p < 0.001$. All tests were for two-tailed calculations, keeping the confidence level at a constant 95%.

Graphical outputs were drawn using GraphPad Prism, ensuring consistency of data interpretation. All the observations followed normal distribution as well as homogeneity of variance, thus validating the robustness of the used statistical tool.

RESULTS

2.4.1 Kisspeptin-10 Inhibits Proliferation of Triple-Negative Breast Cancer Cells

The cytotoxic and anti-proliferative activities of Kisspeptin-10 were investigated in two different types of TNBC cell lines, MDA-MB-231 and MDA-MB-468. The MTT assay was performed to evaluate the activity of Kisspeptin-10 in these cancer cell lines after 24 hours. The tumor cells were incubated with various concentrations of Kisspeptin-10, varying up to the micromolar level.

In MDA-MB-231 cells, a concentration-dependent decrease in cell viability was observed after treatment with Kisspeptin-10. These data showed a typical dose-response relationship typical for a sigmoid curve, confirming the pharmacological reproducibility of the drug's response. From the dose-response curve, half-maximal inhibitory concentration (IC_{50}), required for cell inhibition, was calculated to be 110.21 nM, and IC_{10} was calculated to be 12.13 nM. These data indicated that viability inhibition is mediated by Kisspeptin-10 at low nanomolar concentrations.

For a comparative analysis, Doxorubicin·HCl, as a positive chemotherapeutic agent, has been found to have a higher IC_{50} value of 442.30 nM with a corresponding IC_{10} value of 62.38 nM in the same cell line. Therefore, Kisspeptin-10 has been observed to be fourfold more potent compared with Doxorubicin in inhibiting MDA-MB-231 cell line viability under similar study. Similarly, in the MDA-MB-468 cells, the cytotoxicity potency of Kisspeptin-10 was further increased.

The IC_{50} value was calculated as 88.35 nM, along with an IC_{10} value of 9.31 nM, thereby further validating the sensitization of the basal-like subtype of TNBC cells towards the treatment with Kisspeptin-10. Additionally, the IC_{50} value for Doxorubicin-HCl in the MDA-MB-468 cells was calculated as 378.35 nM, with an IC_{10} value of 39.24 nM, further validating the study. Interestingly, beyond a concentration of 200 nM, Kisspeptin-10 evoked a sharp decrease in cell viability in both cell lines, implying that irreversible cytotoxic or apoptotic pathways might have been initiated.

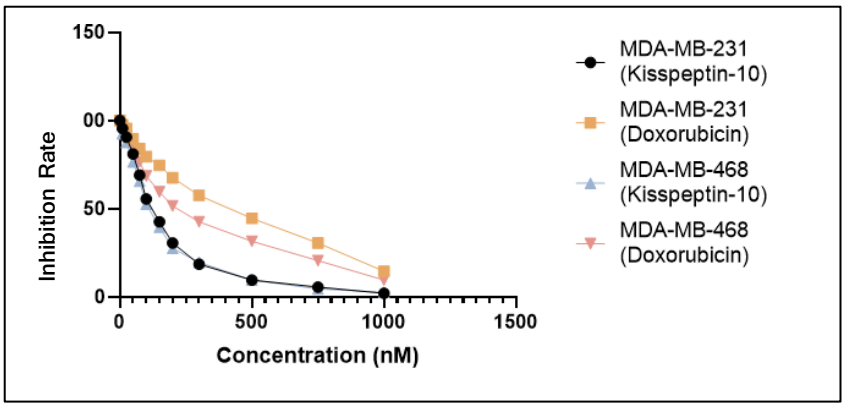

Figure 2.10: *Cell Cytotoxicity assay for MDA-MB-231 and MDA-MB-468 cells.*

2.4.2 Kisspeptin-10 Inhibits Migration and Invasion of Triple-Negative Breast Cancer Cells

The influence of Kisspeptin-10 treatment on the migration ability of triple negative breast cancer cells was investigated in MDA-MB-231 and MDA-MB-468 cell culture line types, which have been assessed in a wound healing assay, a test often utilised as a measure of *in vitro* potential in clinical contexts related to tumour spread, i.e., metastatic potential.

At the initial time point, that is, at 0 h, the wound sizes of all the groups are comparable. This confirmed that all the groups were subjected to uniform scratch wound formation and had the same starting conditions. In the control groups, where no particular treatments had been applied, the MDA-MB-231 and MDA-MB-468 cells had a very rapid migratory response.

In the case of MDA-MB-231, the cells were observed to have undergone a significant decrease in movement when treated with Kisspeptin-10. In the 12-hour time point, the control group displayed significant wound closure, with the K10-treated group showing the least rate of closure, and the K50 group showing minimal movement towards the wound region. The 24-hour point saw the control cells showing the maximum percentage of wound closure, with the Kisspeptin-10 group showing moderate closure and the K50 group showing the least closure with the maximum portion of the wound region unfilled.

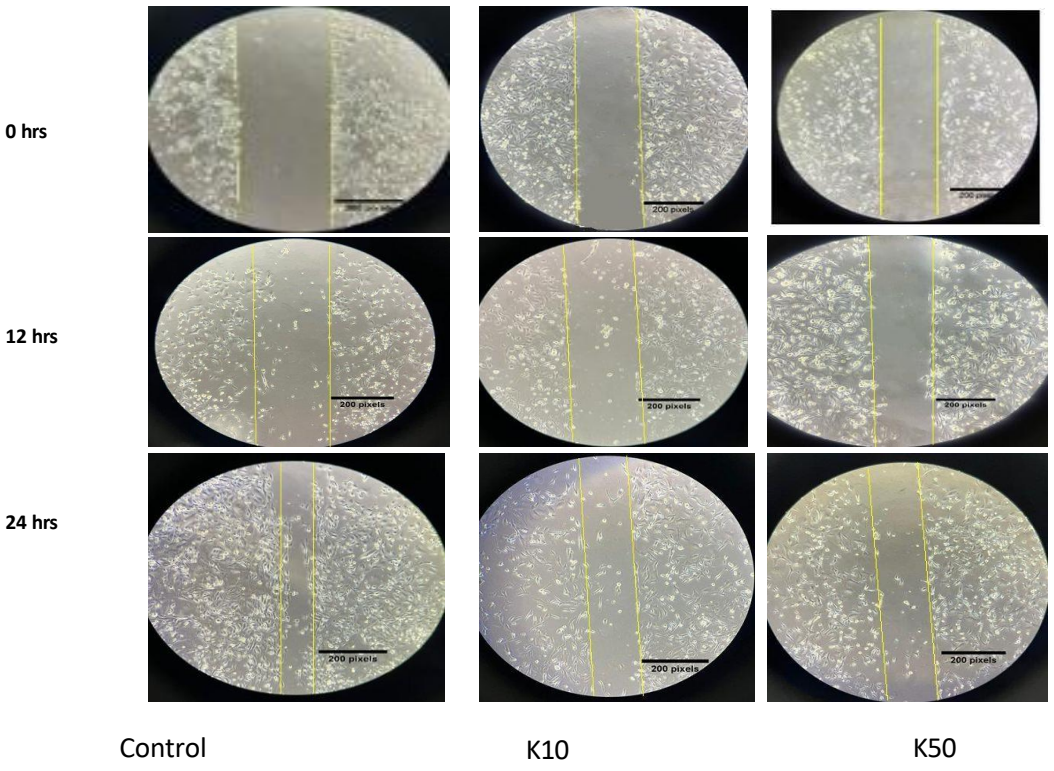

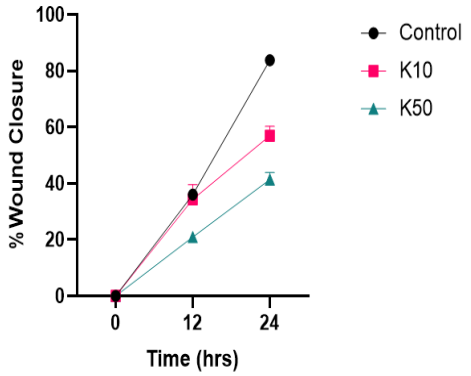

Figure 2.11 *(a) Scratch Wound Assay for MDA-MB-231 cells*

This similar inhibitory trend was evident to an even greater extent with the MDA-MB-468 cells. At the 12-hour mark, it was evident that the control cells were already moving into the gap created by the scratch assay, while both the K10 and K50 cells demonstrated less migration compared to their controls. At the end of the 24-hour mark, while it was evident that the control cells were able to achieve as much as 85% closure compared to their original size in the scratch assay, the K10 cells were able to migrate and achieve about 40%, while the K50 cells were able to migrate to about 25% closure as above.

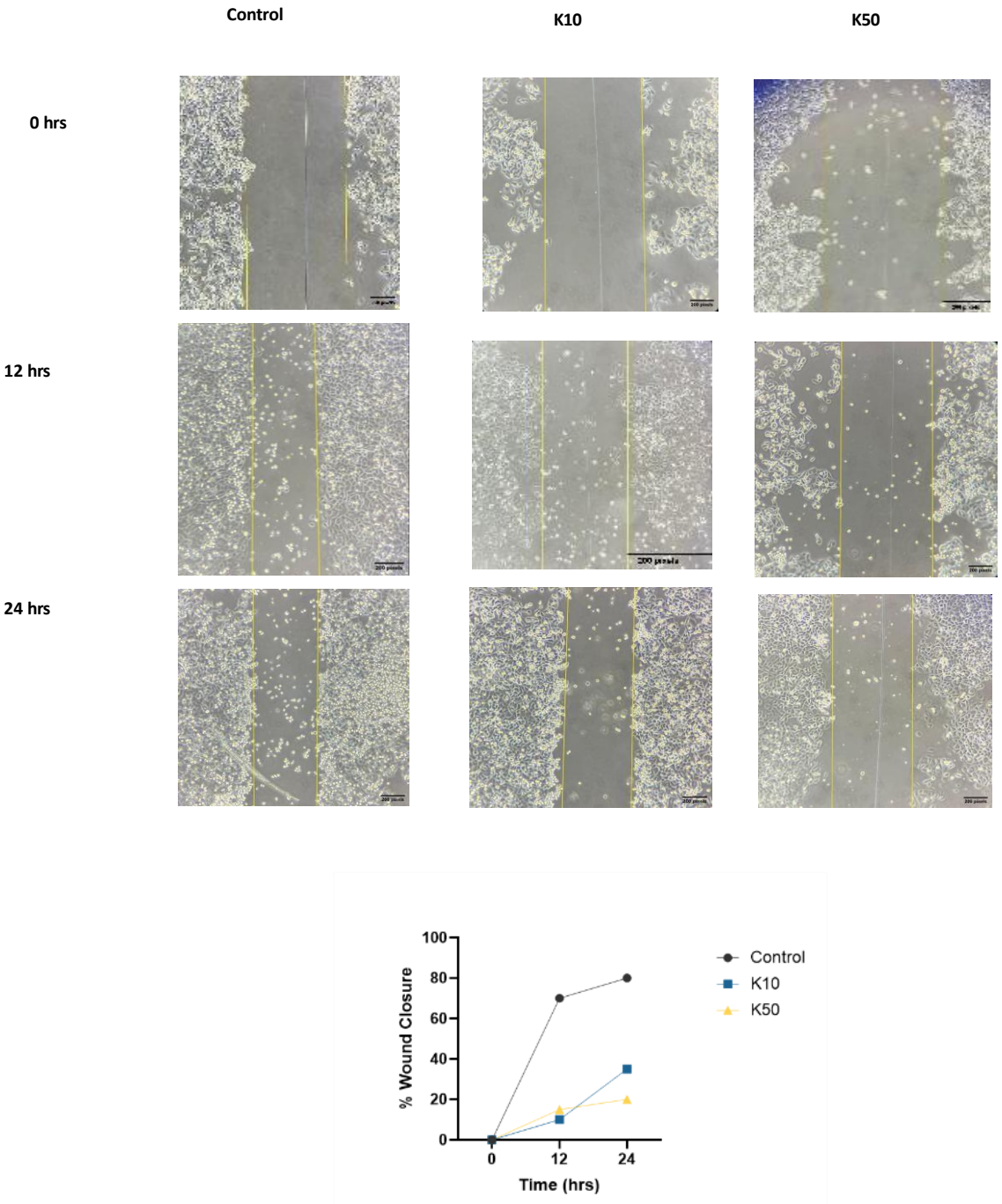

Figure 2.11 *(b) Scratch Wound Assay for MDA-MB-468 cell line.*

The results of the quantitative image-based analysis with the ImageJ computer program supported the finding that the percentage of wound closure was substantially reduced for the two groups of Kisspeptin-treated cells when compared to the untreated cells. The strongest inhibitory effect of Kisspeptin was observed for the K50 cell group. The reproducibility of the study results for two different TNBC cell lines validates the strength of the anti-cell migratory effect of Kisspeptin-10.

Significantly, this inhibitory migration occurred only at K10 and K50 levels; it shows that Kisspeptin-10 does not impair motility as a result of cytotoxic activity but rather acts as a functional modulator of migration behavior. These observations indicate that Kisspeptin-10 is highly potent at attenuating cell motility and could play an important role in addressing the problem of metastasis in TNBCs.

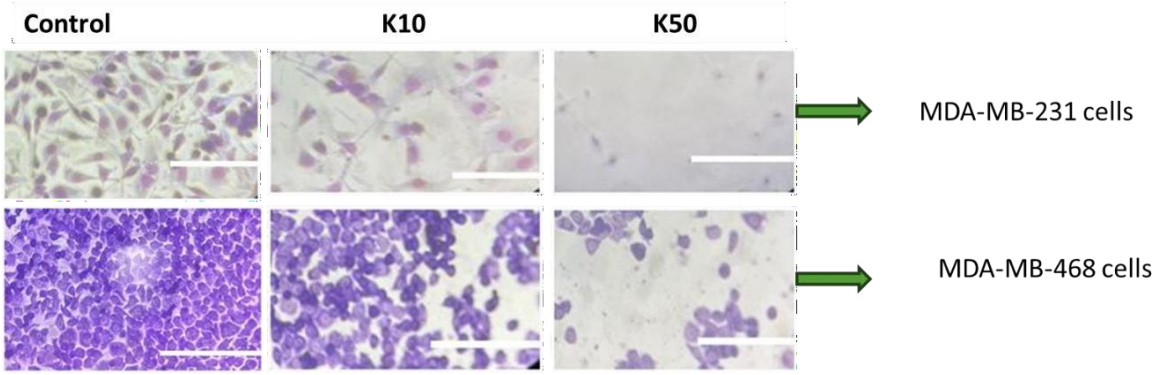

Figure 2.11 *(c) Cell Invasion Assay for MDA-MB-231 and MDA-MB-468 cells (Scale bar indicated 100 µM)*

2.4.3 Kisspeptin-10 Induces Broad Transcriptional Modulation in TNBC Cells

Table 2.14: Nanodrop results for RNA Concentration

Sample	260/280 Ratio	260/230 Ratio	RNA Concentration (ng/µL)
Control	1.92	2.12	612.45
Kisspeptin IC_{10}	2.01	2.09	458.72
Kisspeptin IC_{50}	2.01	2.06	389.54
Doxorubicin IC_{10}	1.99	2.11	421.33
Doxorubicin IC_{50}	2.02	2.07	362.18

Quantitative RT-PCR analyses revealed that Kisspeptin-10 treatment induced significant changes in the transcriptional landscape of TNBC cells. In both MDA-MB-231 and MDA-MB-468 cell lines, exposure to Kisspeptin-10 caused coherent and dose-dependent changes in the expression of transcription factors, EMT regulators, apoptotic mediators, and intracellular signaling molecules.

While both TNBC cell lines responded to Kisspeptin-10, MDA-MB-231 cells consistently showed a higher magnitude of transcriptional modulation than MDA-MB-468 cells. However, the direction of regulation was mostly conserved across the two cell lines.

2.4.3.1 Regulation of Transcription Factor Networks

Kisspeptin-10 significantly modulated the activity of several transcription factors that control cellular differentiation, chromatin modelling, and epithelial–mesenchymal plasticity. The expressions of SP1 in MDA-MB-231 cells increased from the control to 1.07 ± 0.07 at K10 and further to 1.28 ± 0.08 at K50, thus showing progressive transcriptional activation. A similar pattern was also observed for GATA2, which increased to 1.49 ± 0.07 at K10 and to 1.55 ± 0.08 at K50. Similarly, CDX2 expression showed dose-dependent elevation to 1.46 ± 0.07 at K50. In the same vein, FLI1 increased in a dose-dependent manner to reach 1.28 ± 0.06 at K50. Also, NMYC expression was similarly increased, reaching 1.52 ± 0.07 at K50.

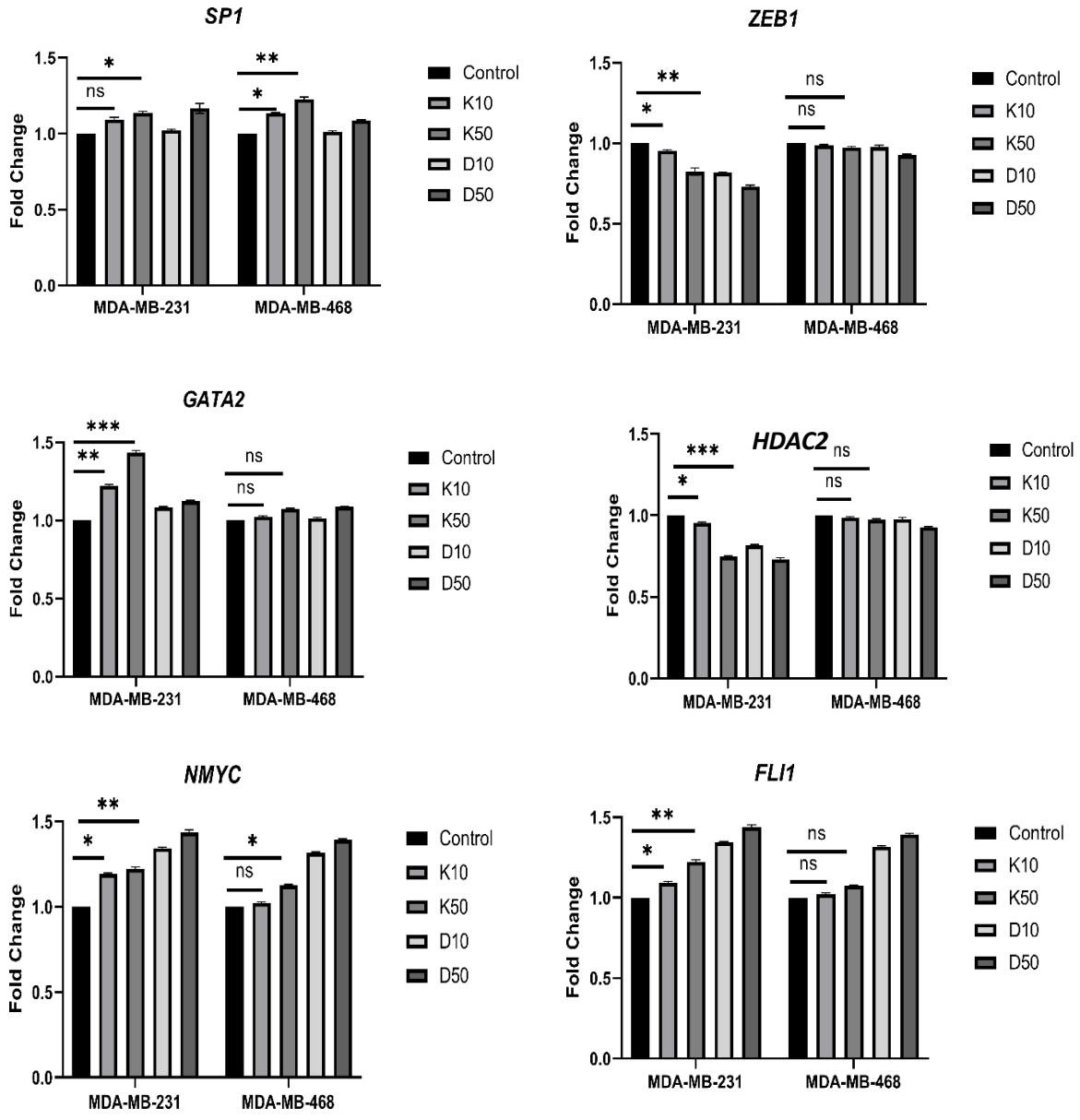

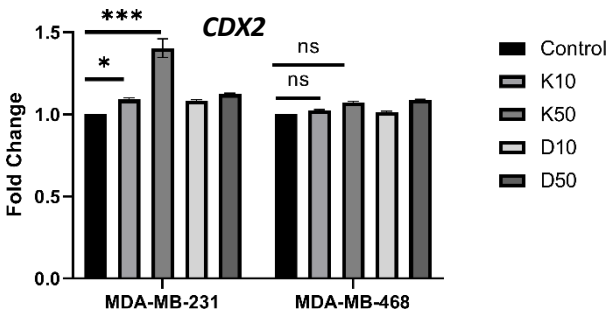

Figure 2.12 (a) Relative Gene Expression of MDA-MB-231 and MDA-MB-468 for transcription factors

In contrast, HDAC2 expression exhibited a gradual decline in the control cells to 0.84± 0.04 at K50, reflecting suppression of chromatin-associated regulatory activity. Similarly, SP1, GATA2, CDX2, NMYC, and FLI1 were also upregulated in MDA-MB-468 cells, although with a comparatively lower magnitude, while HDAC2 expression again showed downregulation to 0.98 ± 0.04 at K50. Importantly, expression of the master inducer of EMT, ZEB1, was markedly repressed in both lines. ZEB1 was downregulated as low as 0.87 ± 0.04 in MDA-MB-231 cells and 0.93 ± 0.05 in MDA-MB-468 cells at K50.

In all, these findings demonstrate that Kisspeptin-10 favours the activation of tumor-suppressive transcription factors and suppresses EMT-associated transcriptional drivers.

2.4.3.2 Reactivation of the KISS1 Signaling Axis

Notably, an evident molecular consequence of Kisspeptin-10 treatment was observed in the potent upregulation of KISS1 and its receptor KISS1R in both TNBC cell lines. In MDA-MB-231, KISS1 was induced to a level of 1.32 ± 0.07 at K10 and to 1.48 ± 0.08 at K50, and KISS1R was induced to 1.38 ± 0.07 and 1.62 ± 0.08, respectively. For MDA-MB-468, KISS1 was induced to 1.22± 0.02.

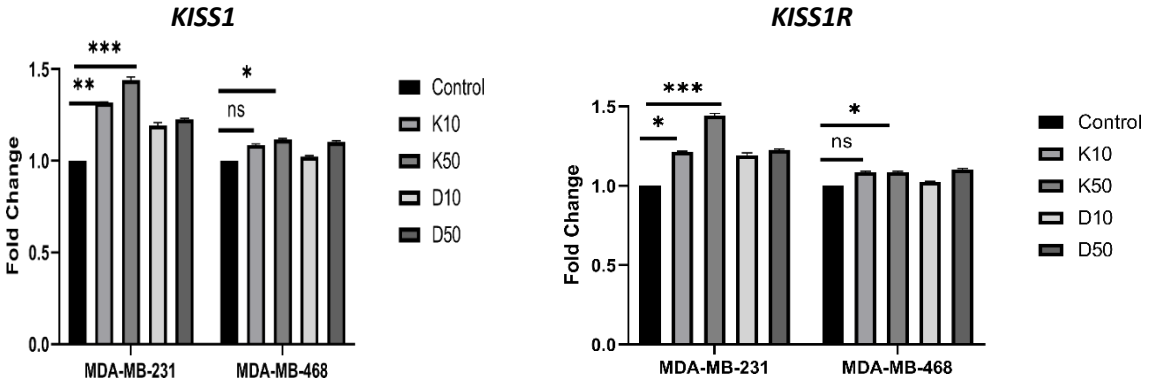

Figure 2.12 (b) Relative Gene Expression of MDA-MB-231 and MDA-MB-468 for KISS1 and KISS1R

2.4.3.3 Kisspeptin-10 Reverses EMT and Modulates Adhesion Markers

Similarly, kisspeptin-10 treatment exhibited significant regulation of EMT and adhesion-related genes. In MDA-MB-231 cells, N-cadherin expression levels decreased from 1 to 0.78 ± 0.04 at K50. Similarly, expression level of CD44 also decreased to 0.79± 0.05. This reduction of mesenchymal and stemness markers. Reduction of vimentin was also highly dose-dependent and had levels of 0.63± 0.04 at K50. In contrast, β-catenin expression was increased to 1.22 ± 0.05, suggesting reinforcement of epithelial adhesion complexes. In MDA-MB-468 cells, similar trends were observed, with N-cadherin decreasing to 0.85 ± 0.05, CD44 to 0.88 ± 0.05, and Vimentin to 0.78 ± 0.05, while β-catenin increased to 1.10 ± 0.05 at K50. The coordinated downregulation of mesenchymal and stemness markers and the upregulation of adhesion-related β-catenin activity clearly delineate the reversal effect Kisspeptin-10 exerts in TNBC via the reversal of EMT phenotype

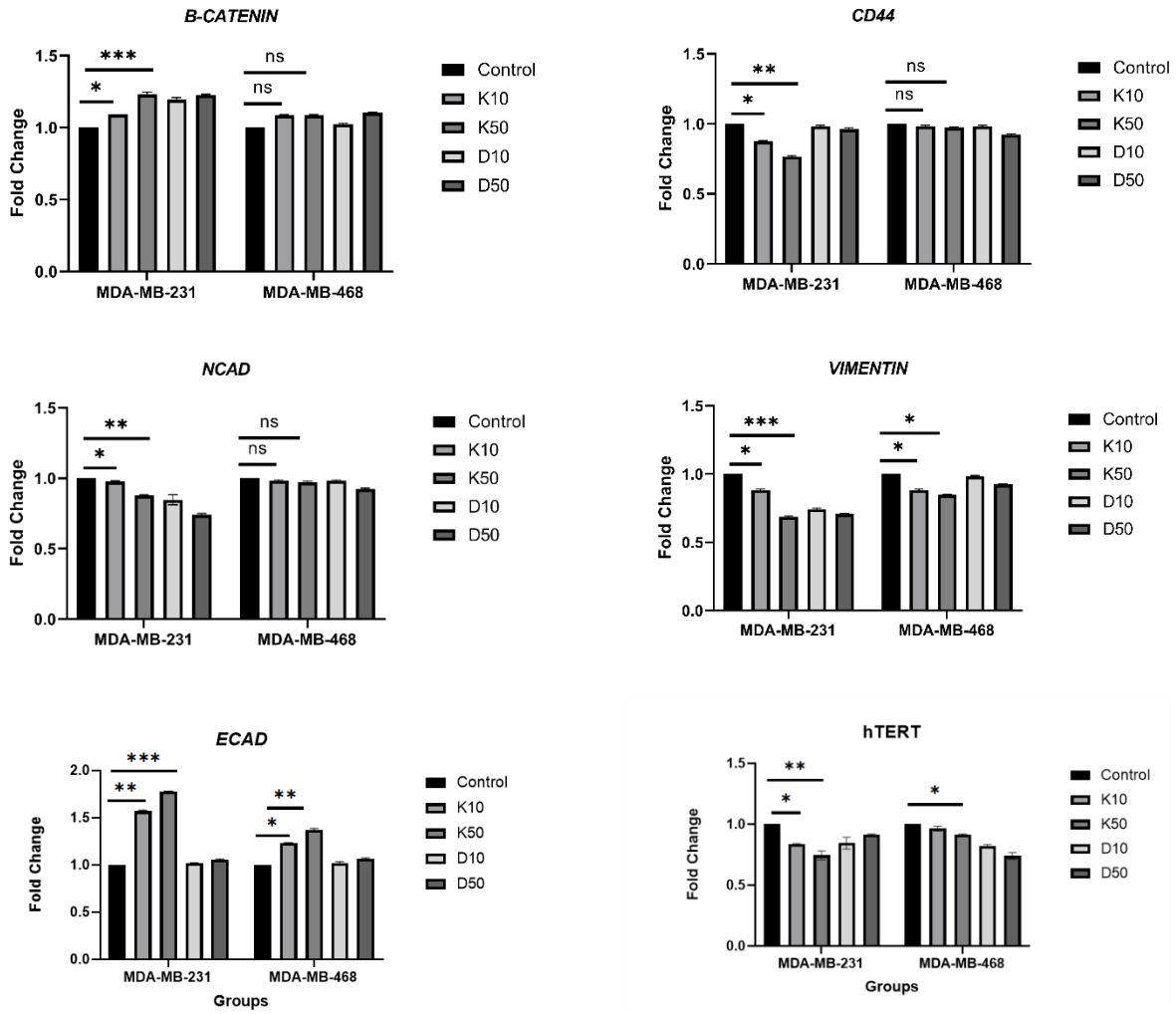

Figure 2.12 (c) Relative Gene Expression of EMT and Adhesion Markers

2.4.3.4 Activation of Apoptotic Gene Networks

Kisspeptin-10 showed strong transcriptional activation of apoptosis-related factors in both TNBC cell lines. In the MDA-MB-231 cell line, the expression of the pro-apoptotic protein BAX increased to 1.32 ± 0.06, CASP3 to 1.38 ± 0.06, and CASP9 to 1.42 ± 0.06 at K50. At the same time, the expression of the anti-apoptotic protein. In MDA-MB-468 cells, although lower levels were achieved, CASP9 increased to 1.30 ± 0.06, CASP3 increased to 1.15 ± 0.05.

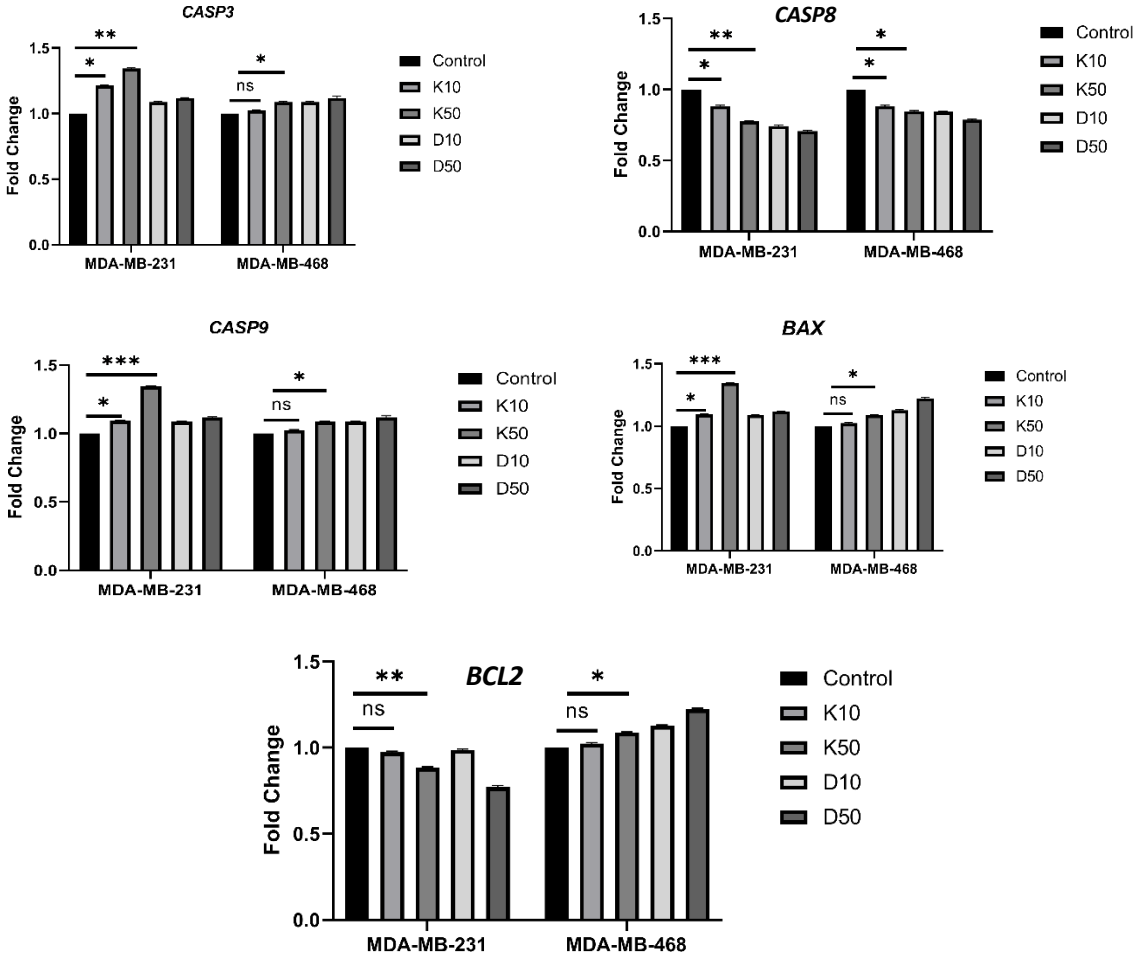

Figure 2.12 (d) Relative Gene Expression of Apoptotic Markers

2.4.3.5 Modulation of Stress, Survival, and Inflammatory Signaling

Kisspeptin-10 significantly regulated multiple intracellular signaling mediators. In MDA-MB-231 cells, PKA expression increased to 1.29 ± 0.05, PKR to 1.37 ± 0.07, and PLCB1 to 1.33 ± 0.06 at K50. On the contrary, CJUN expression was suppressed to 0.79 ± 0.04, reflecting suppression of AP-1-mediated inflammatory and proliferative signaling. PKA increased to 1.44± 0.08, PKR - to 1.45 ± 0.07, PLCB1 - to 1.23 ± 0.06 in MDA-MB-468, while CJUN dropped to 0.82 ± 0.04.

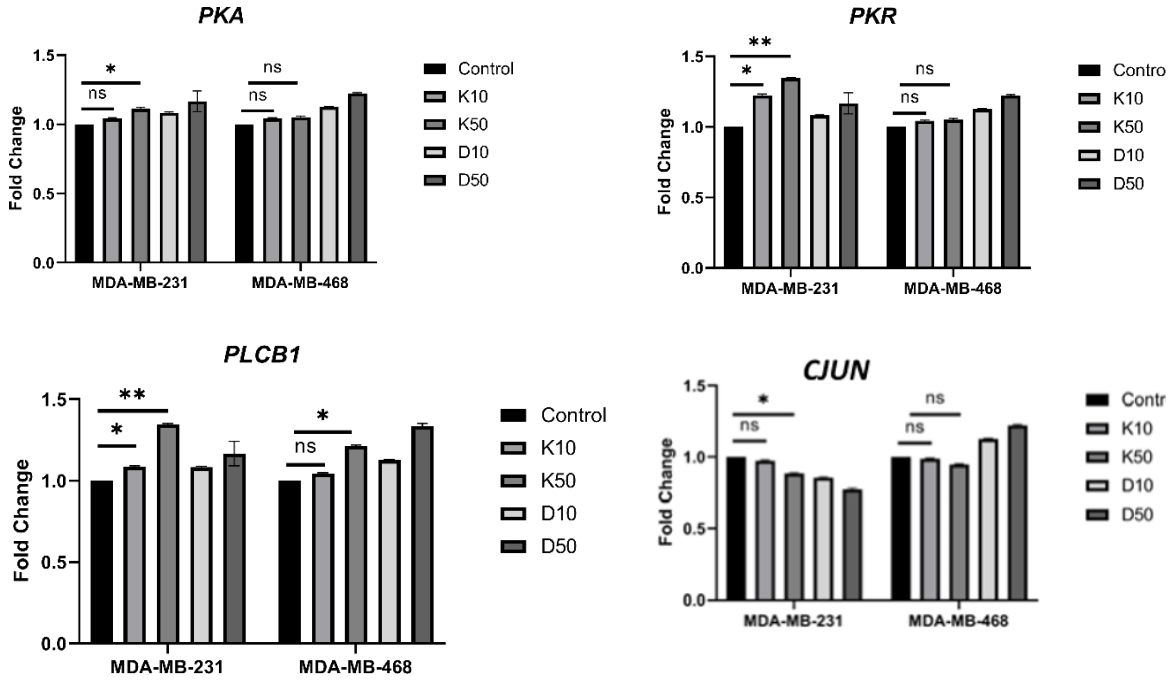

Figure 2.12 (e) Relative Gene Expression of Signalling molecules

Table 2.15: Relative Fold Change Values of Control vs Kisspeptin-Treatment in MDA-MB-231 and MDA-MB-468 cells

Gene	Control	K10-MDA-MB-231	K50-MDA-MB-231	K10-MDA-MB-468	K50-MDA-MB-468
SP1	1	1.07 ± 0.07	1.28 ± 0.08	1.22 ± 0.06	1.42 ± 0.07
GATA2	1	1.29 ± 0.07	1.55 ± 0.08	1.30 ± 0.06	1.48 ± 0.07
CDX2	1	1.25 ± 0.06	1.46 ± 0.07	1.10 ± 0.05	1.25 ± 0.06
NMYC	1	1.23 ± 0.07	1.52 ± 0.07	1.18 ± 0.06	1.38 ± 0.07
FLI1	1	1.15 ± 0.05	1.28 ± 0.06	1.05 ± 0.05	1.18 ± 0.06
HDAC2	1	0.95 ± 0.05	0.84 ± 0.04	0.94 ± 0.06	0.85 ± 0.04
ZEB1	1	0.88 ± 0.04	0.87 ± 0.04	0.92 ± 0.05	0.80 ± 0.05
KISS1	1	1.32 ± 0.07	1.48 ± 0.08	1.30 ± 0.06	1.22 ± 0.02
KISS1R	1	1.38 ± 0.07	1.62 ± 0.08	1.25 ± 0.06	1.48 ± 0.07
N-Cadherin	1	0.88 ± 0.04	0.78 ± 0.04	0.92 ± 0.05	0.85 ± 0.05
CD44	1	0.90 ± 0.04	0.79 ± 0.05	0.95 ± 0.05	0.88 ± 0.05
β-Catenin	1	1.08 ± 0.05	1.22 ± 0.05	1.05 ± 0.05	1.10 ± 0.05
Vimentin	1	0.85 ± 0.04	0.63 ± 0.04	0.92 ± 0.05	0.78 ± 0.05

BAX	1	1.08 ± 0.05	1.32 ± 0.06	1.02 ± 0.05	1.08 ± 0.05
BCL2	1	0.92 ± 0.04	0.85 ± 0.05	1.07 ± 0.05	1.13 ± 0.05
CASP3	1	1.10 ± 0.05	1.38 ± 0.06	1.05 ± 0.05	1.15 ± 0.05
CASP8	1	1.05 ± 0.05	1.22 ± 0.06	1.02 ± 0.05	1.12 ± 0.05
CASP9	1	1.18 ± 0.05	1.42 ± 0.06	1.10 ± 0.05	1.30 ± 0.06
PKA	1	1.12 ± 0.06	1.29 ± 0.07	1.23± 0.06	1.45 ± 0.07
PKR	1	1.15 ± 0.06	1.37 ± 0.07	1.18 ± 0.06	1.35 ± 0.07
PLCB1	1	1.10 ± 0.05	1.33 ± 0.06	1.08 ± 0.05	1.22 ± 0.06
CJUN	1	0.98 ± 0.05	0.79 ± 0.04	0.95 ± 0.09	0.83± 0.04
HTERT	1	0.83±0.01	0.72±0.05	0.98±0.02	0.92±0.01

2.4.3.6 Survival Association of Transcription Factors

High expression of many Kisspeptin-regulated transcription factors showed significant associations with survival outcomes in patients. While SP1 expression showed a strong favorable prognostic association, with significantly improved overall survival for high levels of SP1 (HR = 0.62, CI: 0.49–0.79, $p < 0.001$), GATA2 expression showed markedly improved survival probability as well (HR = 0.47, CI: 0.37–0.59, $p < 0.001$).

Expression of FLI1 also related to better survival HR = 0.79, CI: 0.64–0.99, $p = 0.042$, and overexpression of ZEB1 was found in association with higher survival rates HR = 0.69, CI: 0.60–0.81, $p < 0.001$. By contrast, the expression of HDAC2 was strongly and negatively associated with prognosis, as high HDAC2 was significantly associated with low survival (HR = 1.65, CI: 1.49-1.83, $P < 0.0001$). A modest yet significant adverse survival association was seen for the expression of the MYCN oncogene. CDX2 expression was found not to exhibit statistically significant association with the survival of the patients.

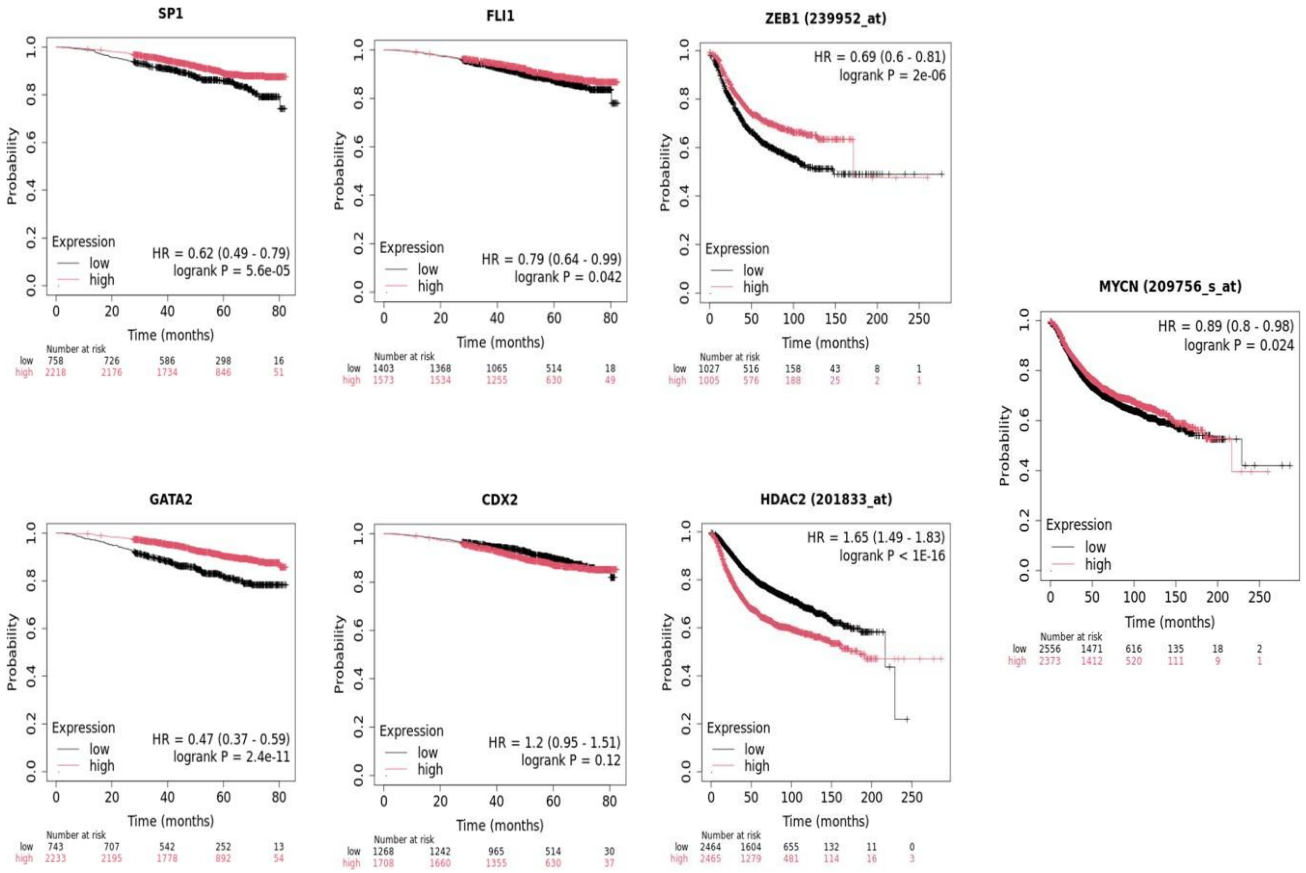

Figure 2.13 *(a) Survival analysis of Transcription Factors*

2.4.3.7 Survival Association of EMT and Adhesion Markers

Among these was the Kaplan–Meier analysis showing that both epithelial and mesenchymal markers also have prognostic associations. High expression of CDH1 (E-cadherin) was significantly associated with improved overall survival HR = 1.20, CI: 0.76–0.93, p = 0.00036, and thus supported its protective epithelial role. On the other hand, high expression of CDH2 (N-cadherin) was significantly associated with lower survival probability HR = 1.13, CI: 1.02–1.25, p = 0.021. Vimentin expression showed a nonsignificant trend toward favorable prognosis, with a hazard ratio of 0.92, CI: 0.83–1.02, p = 0.095, indicating possible subtype-dependent variability. CTNNB1 expression did not show significant survival associations, HR = 1.02, CI: 0.87–1.18, p = 0.84. Moreover, the expression of CD44 showed a significant relation with better survival rate: HR = 0.78, CI: 0.67–0.91, p = 0.0015.

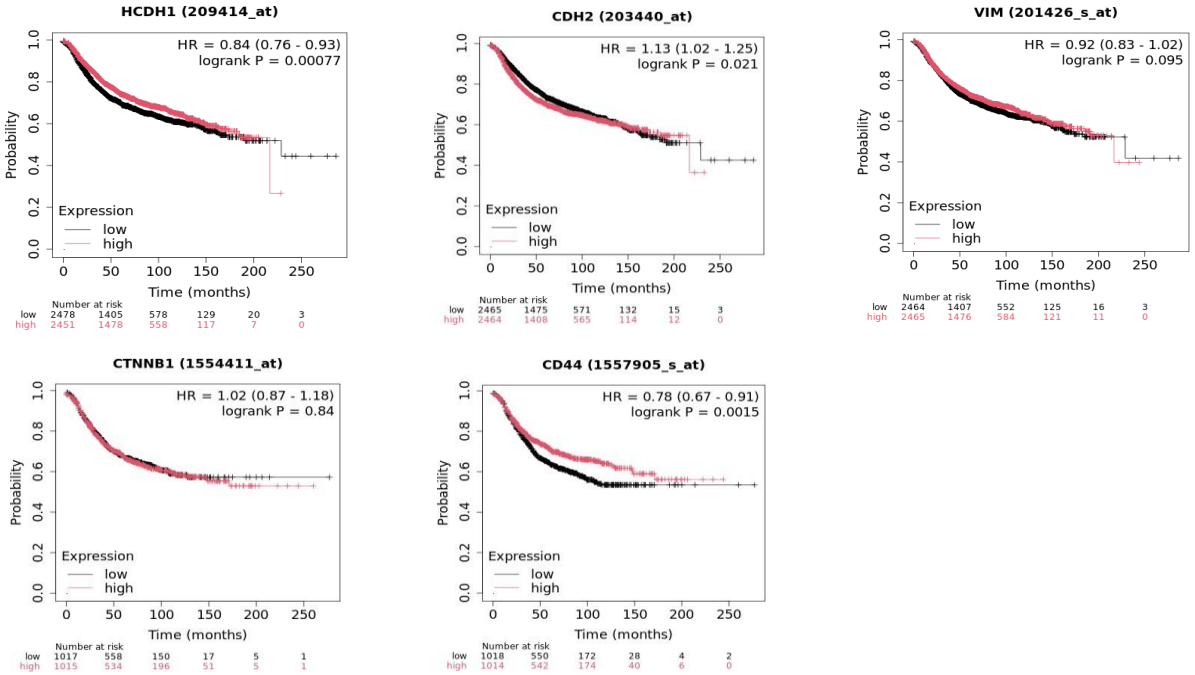

Figure 2.13 *(b) Survival analysis of EMT markers and adhesion markers*

2.4.3.8 Survival Association of Apoptotic Markers

Apoptotic genes exhibited various types of prognoses. High BCL2 level was significantly related to OS. The HR = 0.73, CI = 0.66–0.81, and p = 1.2×10^{-9}. CASP9 level was significantly related with favorable prognosis. The HR = 0.63, CI = 0.57–0.70. By contrast, the expression of CASP3 was strongly linked with worse survival outcome results, with a hazard ratio of 1.27, a CI of 1.15-1.41. No statistically significant associations of CASP8 and BAX with OS were detected (HR = 0.95; p = 0.36 and HR = 1.06; p = 0.28, respectively). This study highlights the different prognostic importance of regulators of apoptosis in breast cancer.

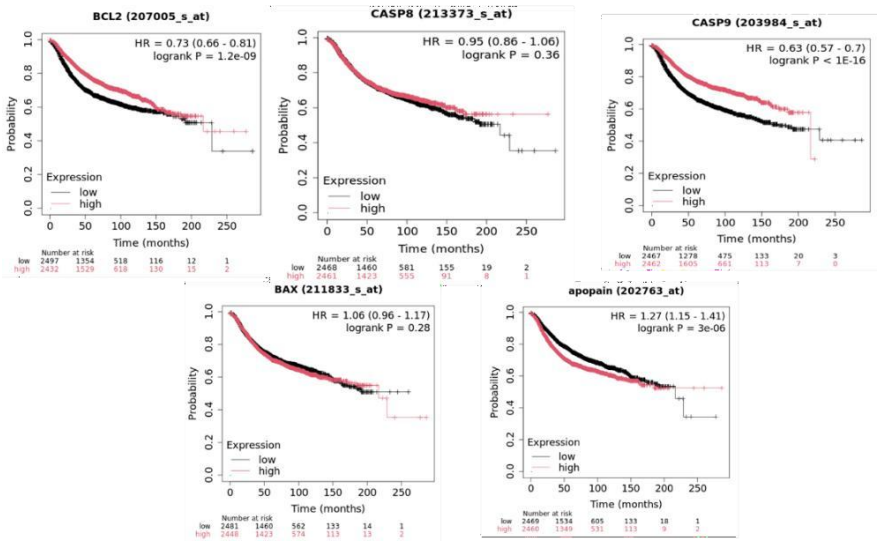

Figure 2.13 *(c) Survival analysis of Apoptotic markers*

2.4.3.9 Survival Association of Signaling Molecules

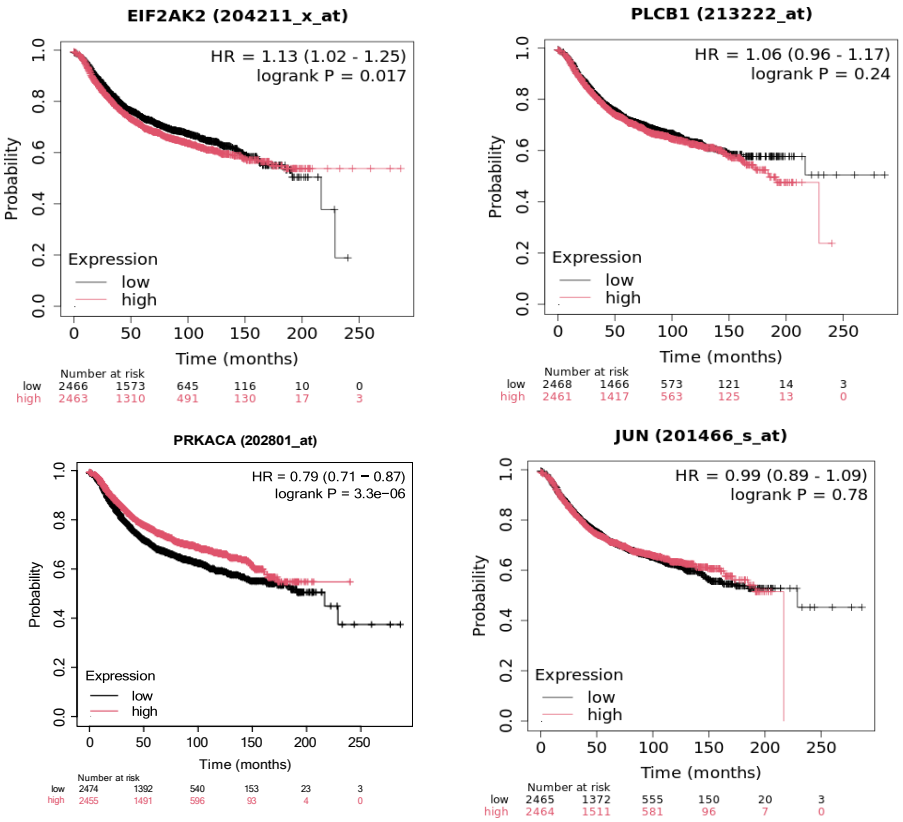

Figure 2.13 *(d) Survival analysis of Signalling molecules*

Among these signaling regulators, EIF2AK2 (PKR) showed a significant association with poor overall survival with HR = 1.13, CI: 1.02–1.25, p = 0.017, thus showing its probable prognostic value. In contrast, PLCB1 = 1.06, 95% CI: 0.96–1.17, p = 0.24 and JUN = 0.99, 95% CI: 0.89–1.09, p = 0.78 did not show significant survival correlations.

2.4.4 Metabolomic Profiling

2.4.4.1 Global Metabolomic Alterations Induced by Kisspeptin-10

Untargeted LC-MS metabolomic approach was employed to assess the biochemical effects associated with Kisspeptin-10 treatment in the MDA-MB-231 cell line. A comparative analysis of the control group and K10 and K50 treated cells revealed that the levels of all the metabolites are affected substantially after Kisspeptin-10 treatment.

The volcano plot showed the overall distribution of significantly changed metabolites across both IC_{10} and IC_{50}-treated states, from which there is an increased number of metabolites found under IC_{50}. Various metabolites like Gingerdiol/Norcapsaicin, Usambarensine, S-Prenyl-L-cysteine, peptide-like compounds, and Tetrahydropterins were found entirely lacking in controls and present in all treated states. On the other hand, metabolites such as DL-Tryptophan, Cadaverine, Octopamine, and L-

Isoleucine/L-Leucine were found in all the experimental groups but with significant variations in abundance

These results reveal the role of Kisspeptin-10 in the occurrence of perceptible metabolic changes.

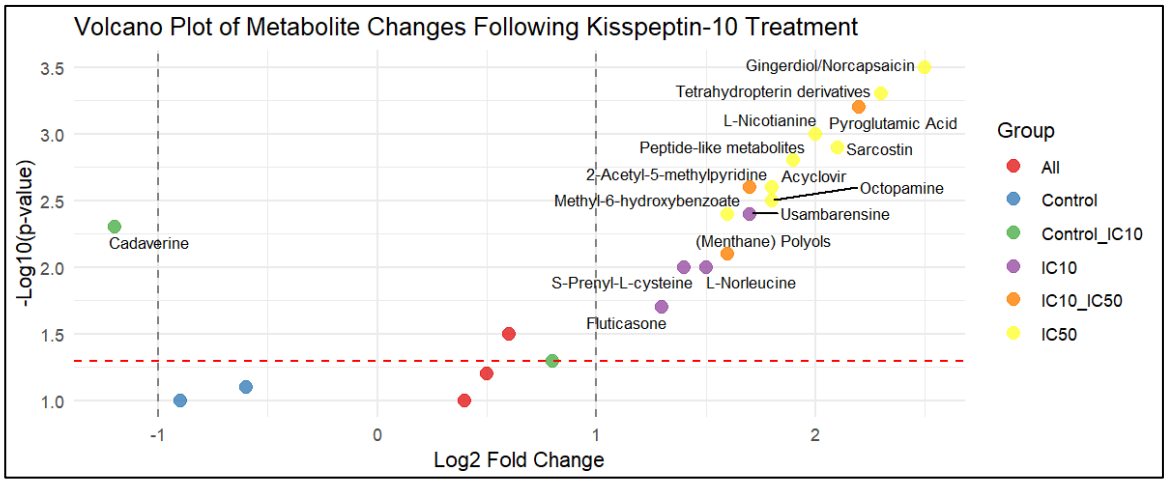

Figure 2.14 a) *Volcano plot depicting log_2 fold change versus $–log_{10}$(p-value) of metabolite abundance in IC_{10} and IC_{50} Kisspeptin-10-treated cells compared to control. Several significantly altered metabolites, including Gingerdiol/Norcapsaicin, Peptide-like metabolites, L-Norleucine, and Acyclovir, are annotated.*

2.4.4.2 Pathway Enrichment Analysis of Altered Metabolites

The enrichment pathways indicated that metabolites regulated by Kisspeptin-10 were significantly enriched in angiogenesis-related pathways, anti-proliferative pathways, where the enrichment ratio was the strongest, anti-proliferative pathways, and cytotoxicity-related pathways, as well as glutathione-related pathways, followed by pathways related to apoptosis-associated ones. Again, moderate enrichments were also observed for amino acid metabolism, biosynthesis of the natural alkaloids, and the metabolic pathways of the nucleotides and purines. The enriched metabolism pathways point to the induction of the metabolic response caused by Kisspeptin-10, covering cell survival, the metabolism of the antioxidant defense system, and the biosynthetic metabolism.

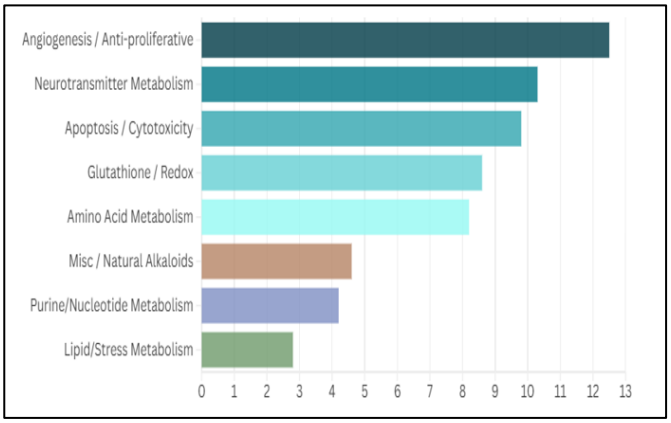

Figure 2.14 b) *Bar plot of top enriched biological themes and pathways classified by metabolite function, including angiogenesis/anti-proliferative, neurotransmitter metabolism, apoptosis/cytotoxicity, and glutathione/redox metabolism, with the number of metabolites involved shown on the x-axis.*

2.4.4.3 Compound–Pathway Relationship Analysis

To refine the identification of compound contributions at the level, a Sankey plot-style compound-pathway flow visualization was constructed. This showed that both DL-Tryptophan and Octopamine contributed to several enriched pathways, reinforcing their important roles in cell metabolism. A series of amino acid-derivative compounds, including L-Isoleucine/L-Leucine, L-Norleucine, and S-Prenyl-L-cysteine, were highly enriched in amino acid-related metabolism, reflecting the remodeled protein and amino acid metabolism.

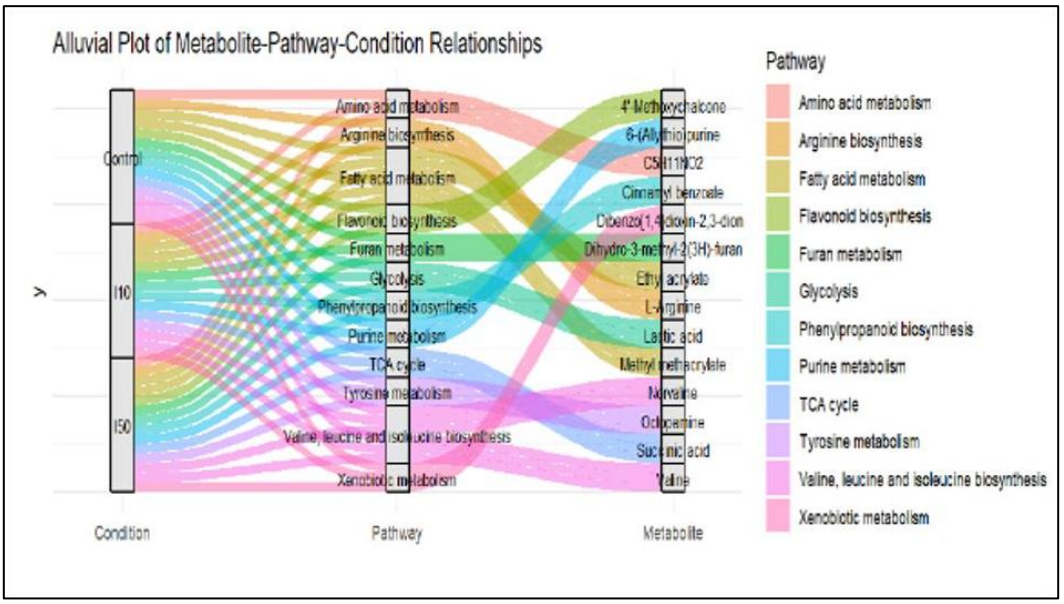

Figure 2.14 c) *Alluvial plot linking experimental conditions (Control, IC_{10}, IC_{50}) to affected pathways and specific metabolites, highlighting pathway shifts associated with Kisspeptin-10 treatment.*

The alluvial plot showed distinct associations among experimental conditions (Control, K10, and K50), altered metabolic pathways, and their respective metabolites. Kisspeptin-10 treatment at both the IC_{10} and IC_{50} concentrations was associated with a differential regulation of pathways related to amino acid metabolism, fatty acid metabolism, glycolysis, the TCA cycle, and purine metabolism.

Metabolites like L-valine, succinate, uracil, fumarate, and citric acid were significantly enriched in Kisspeptin-treated groups, especially under the K50 condition, suggesting an increased metabolic flux through the TCA cycle and amino acid biosynthetic pathways. Further, it is obvious that xenobiotic and flavonoid metabolism was linked more specifically with Kisspeptin-10 exposure, thus pointing to the activation of detoxification and stress-response metabolic mechanisms.

2.4.4.4 Metabolite–Pathway Network Analysis

The pathway-metabolite association network demonstrated the critical association of significantly altered metabolites with their corresponding biological pathways. Usambarensine and Indoleacrylic acid were predominantly associated with purine and nucleotide metabolism, indicating modulated biosynthesis and turnover of nucleic acid. Pyroglutamic acid, 2-Acetyl-5-methyl-pyridine, and Fluticasone were associated with glutathione and antioxidant pathways, suggesting metabolic regulation sensitive to redox.

Metabolites like Methyl 2-(10-heptadecenyl)-6-hydroxybenzoate, derivatives of polyol, and Sarcostin could be categorized under cytotoxicity and metabolic processes associated with cell death, further strengthening the pro-apoptotic effect identified at the transcriptional level.

Taken together, these metabolite-pathway relationships indicate that Kisspeptin-10 acts to stimulate a biochemically coordinated response through metabolic pathways that regulate cell survival, redox balance, neurotransmitter metabolism, and antiproliferative signaling.

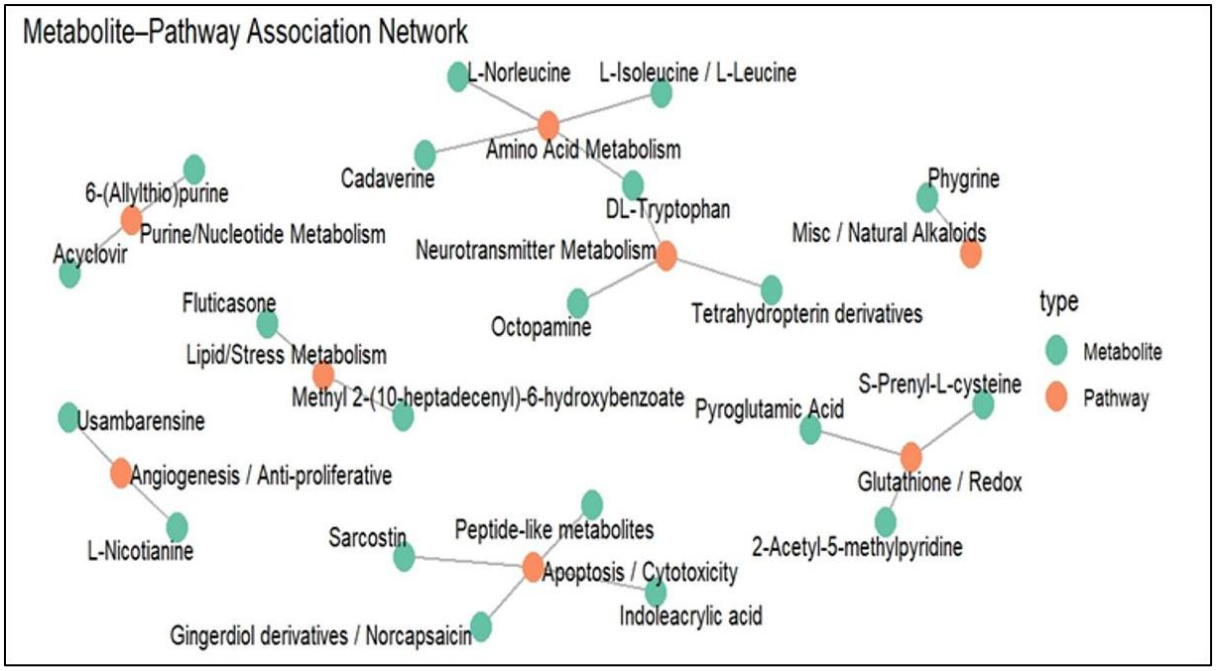

Figure 2.14 d) *Metabolite–pathway association network showing interactions between significantly altered metabolites and their corresponding metabolic pathways. Colored nodes represent either metabolites (green) or pathways (orange), providing a visual overview of metabolomic reprogramming upon Kisspeptin-10 exposure.*

2.4.5 In Silico Transcriptomic Validation

2.4.5.1 Dataset Selection and Overview

To affirm the experimental data from a clinical and molecular standpoint, publicly available transcriptomic datasets were downloaded from the NCBI Gene Expression Omnibus Database. Two publicly available datasets possess the qualifications necessary for our purpose: GDS4069 and GDS825 contain well-annotated triple negative breast cancer data as well as non-triple negative breast cancer data, making them suitable for determining the degree to which the *in vitro* transcriptional profile changes induced by treatment with Kisspeptin-10 translate into patient sample datasets.

Preprocessing and normalization were carried out to ensure the elimination of technical variation and reliable comparison between sample groups. The values were transformed using the base 2 logarithm, and then the probes were annotated with unique gene symbols, keeping the most representative probes per gene. Filtering out low-expression genes helps in eliminating noise and making the data more biologically relevant.

2.4.5.2 Identification of Differentially Expressed Genes (DEGs)

Differential gene expression analysis was conducted to assess differential expression between TNBC and non-TNBC BC samples, using statistical thresholds of a |log2 fold change|>1 and an adjusted p-

value< 0.05. It was identified that the "Volcano Plot" visualization confirmed that there is highly symmetrical expression between upregulated and downregulated genes, validating the high level of transcriptional divergence between the TNBC and non-TNBC. The key upregulated genes in TNBC include SPARC, GDF15, KLK11, TCF19, and GAS2. They play a part in the modulation of the extracellular matrix, stress responses, invasiveness, and transcription On the contrary, some of the significantly downregulated genes that have critical roles are CDH1 or E-cadherin, CDH8, SLC22A18AS, MAP1B, and RARFG3.

And when the two sets of data were used for cross-comparison, approximately 70 consistently dysregulated genes were obtained to constitute the high confidence TNBC transcription signature.

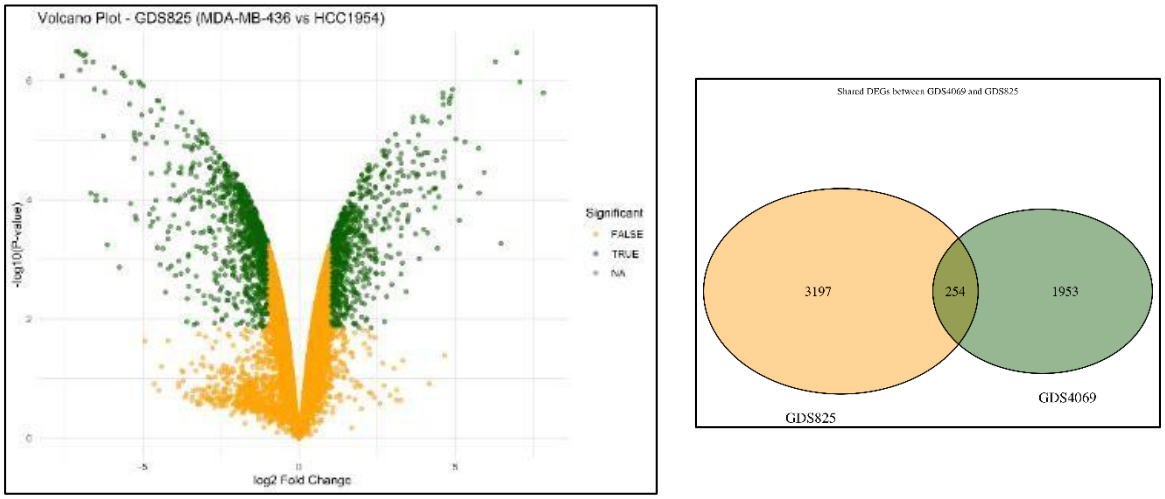

Figure 2.15 a) *Volcano plot of DEGs from GDS825 (MDA-MB-436 vs. HCC1954), showing the distribution of genes based on log_2 fold change and statistical significance (adjusted p-value). Green points indicate significantly differentially expressed genes. Venn diagram illustrating the overlap of DEGs between datasets GDS825 and GDS5099. A total of 234 DEGs were shared and used for downstream analyses.*

2.4.5.3 Hierarchical Clustering and Heatmap Analysis

A hierarchical clustering for the shared DEGs was performed using the z-score normalization method, which yielded a clear and reproducible distinction between the TNBC group and the non-TNBC group.

The heatmap established that the data strongly cluster with regards to characteristics of upregulation of genes related to migration, stress adaptation, and plasticity of transcription, and the corresponding downregulation of epithelial and differentiation-related genes.

Genes like GAS2, FGB, RARFG3, and SLC1A1 were found with strong upregulation in the TNBC samples, while genes like ECAD (CDH1), MAP1B were found to be downregulated.

These clusters further reaffirmed the fact that TNBC retains a unique and consistent transcriptomic profile through the regulation of coordinated programs.

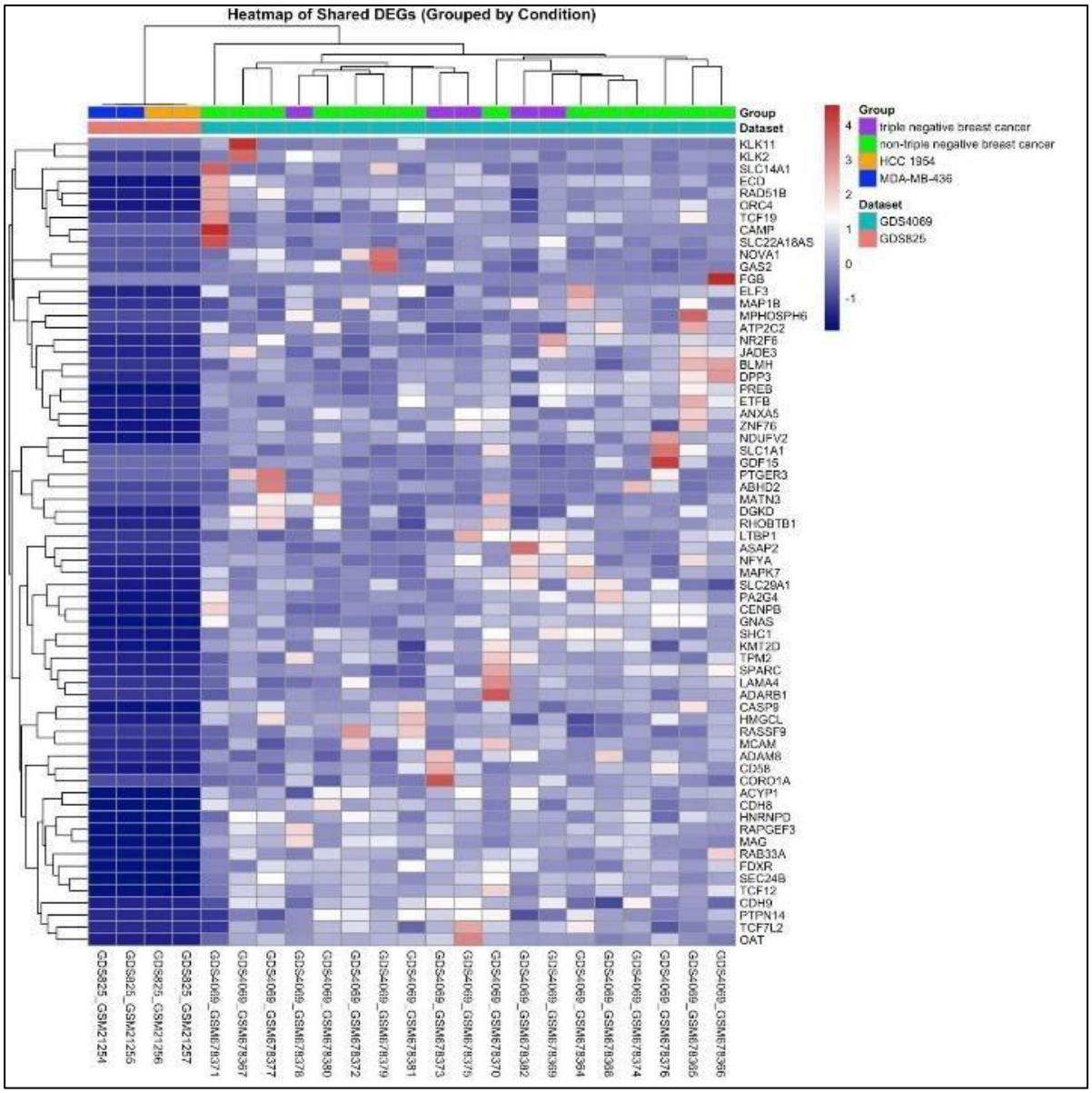

Figure 2.15 *(b) Heatmap of shared DEGs depicting expression profiles across TNBC (MDA-MB-436) and non-TNBC (HCC1954) samples. Samples are grouped by condition, and gene expression is scaled and clustered. Red indicates upregulation, and blue indicates downregulation.*

2.4.5.4 Construction of Gene–Regulator Network

A bipartite gene-regulator interaction network was implemented with the help of Cytoscape software. A list of 20 transcription factors and regulators was compiled on the basis of literature surveys as well as data retrieved from the TFLINK database, with emphasis on genes related to the regulation of gene expression, EMT, apoptosis, chromatin remodeling, etc.

Network analysis showed SP1 to play a major regulatory function by connecting to eight DEGs: “This highlights SP1's major contribution to TNBC transcription regulation.” Moreover, the connectivity

between ZEB1 and other genes related to epithelial suppression and cytoskeleton reorganization reinforced its ability to promote EMT.

HDAC2 interacted with various genes, such as genes in chromatin regulation, linking epigenetics to TNBC. Decreased connectivity of the pro-apoptotic regulator genes CASP3, CASP8, and BAX and their target genes indicated attenuated apoptotic pathways in TNBC tumors. Additional regulatory nodes such as KMT2D and TCF12 were involved in chromatin remodeling and transcriptional control, highlighting extensive epigenetic reprogramming in TNBC. Further, the node size-based degree analysis confirmed the core regulatory triad of SP1, ZEB1, and HDAC2 in the transcriptional landscape of TNBC.

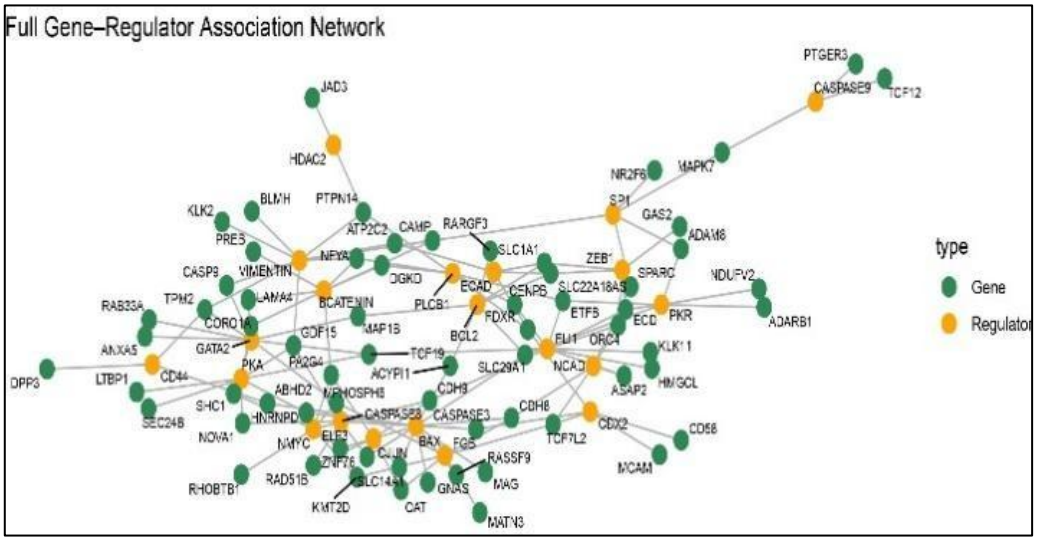

Figure 2.15 c): *Gene–Regulator Association Network constructed from shared DEGs across GDS825 and GDS5099 datasets. Orange nodes represent regulatory factors (e.g., SP1, GATA2, ZEB1, HDAC2), and green nodes represent target genes. Edges denote regulatory interactions, highlighting transcriptional hubs in TNBC.*

2.4.6 miRNA Expression Analysis in TNBC Cell Lines

Expression of miR-345-3p, miR-200c-3p, and miR-577 was quantified in MDA-MB-231 and MDA-MB-468 cells following treatment with Kisspeptin-10 at IC_{10} (K10) and IC_{50} (K50) and compared with Doxorubicin controls (D10 and D50). All values were normalized to U6 and expressed relative to untreated control.

2.4.6.1 miR-345-3p Expression

In MDA-MB-231 cells, miR-345-3p expression was significantly higher upon Kisspeptin-10 treatment. A fold change in control to 1.22 ± 0.04 at K10 and a further increase to 1.35 ± 0.05 at K50 show a clear induction in a dose-dependent manner.

miR-345-3p in MDA-MB-468 cells had very little change in expression. K10 treatment incurred a fold change of 1.05 ± 0.04, and K50 had 1.08 ± 0.04; these are not radically different from the control. Doxorubicin-treated groups also showed very slight changes in 1.00 ± 0.03 at D10 and 1.02 ± 0.04 at D50.

Results showed that Kisspeptin-10 induced the expression of miR-345-3p primarily in MDA-MB-231 cells, while MDA-MB-468 cells were relatively resistant to miR-345-3p modulation.

2.4.6.2 miR-200c-3p Expression

Expression of miR-200c-3p is strongly and significantly upregulated in a dose-dependent manner in response to Kisspeptin-10 treatment in MDA-MB-231 cells. Expression significantly increased from 1.00 ± 0.05 in the control to 1.35 ± 0.05 at K10 and further to 1.55 ± 0.06 at K50. There was only a mild elevation after treatment with Doxorubicin, 1.08 ± 0.04 at D10 and 1.10 ± 0.04 at D50.

In contrast, MDA-MB-468 cells had minimal changes in miR-200c-3p expression. K10 resulted in 1.08 ± 0.04 and K50 showed 1.05 ± 0.04, which were insignificantly different from control; doxorubicin groups also remained near baseline.

Therefore, miR-200c-3p strongly responds to Kisspeptin-10 in MDA-MB-231 cells but stays almost the same in MDA-MB-468 cells.

2.4.6.3 miR-577 Expression

Upon Kisspeptin-10 treatment in the case of MDA-MB-231 cells, microRNA-577 expression revealed an increase albeit minimal in nature. This increase was noticed by an increase in fold change values rising from 1.00 ± 0.05 for the control to 1.08 ± 0.04 for the K10-treated cells and to 1. In MDA-MB-468 cancer cells, the level of miR-577 did not substantially vary across all treatment conditions. The level in the K10 and K50 conditions was 1.05 ± 0.04 and 1.08 ± 0.04, respectively.

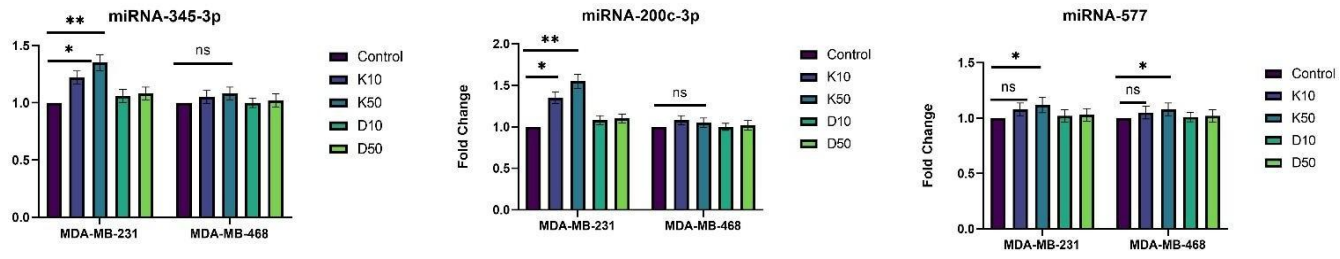

Figure 2.16): *miRNA expression Analysis of Control vs Kisspeptin-10 treated groups for both the cell lines.*

2.4.7 Western Blot Analysis

Protein expression changes induced by Kisspeptin-10 were validated by Western blotting in MDA-MB-231 and MDA-MB-468 cells treated with IC_{10} (K10) and IC_{50} (K50) concentrations. Band intensities were normalized to β-actin and expressed relative to untreated control.

2.4.7.1 Transcription Factor Proteins

In MDA-MB-231 cells, SP1 protein expression increased from 1 in control to 1.02 ± 0.06 at K10 and further to 1.28 ± 0.07 at K50. Similarly, GATA2 increased to 1.20 ± 0.07 at K10 and 1.42 ± 0.08 at K50. While CDX2 rose to 1.08 ± 0.06 at K10 and further to 1.22 ± 0.06 at K50, FLI1 increased to 1.02 ± 0.05 and 1.28 ± 0.06, respectively. Strikingly, the protein expression of NMYC was highly induced at 1.10 ± 0.06 at K10 and 1.55 ± 0.07 at K50. Moreover, ZEB1 protein levels decreased drastically to 0.82 ± 0.04 at K10 and further to 0.62 ± 0.04 at K50.

In MDA-MB-468 cells, SP1 increased to 1.18 ± 0.06 at K10 and 1.05 ± 0.06 at K50. GATA2 increased to 1.25 ± 0.06 and 1.02 ± 0.07, CDX2 to 1.02 ± 0.05 and 1.09± 0.06, FLI1 to 1.05 ± 0.05 and 1.08 ± 0.06, and NMYC to 1.02 ± 0.06 and 1.09 ± 0.06 at K10 and K50, respectively. HDAC2 decreased to 0.92 ± 0.05 at K10 and 0.85 ± 0.04 at K50, while ZEB1 declined to 0.90 ± 0.05 and 0.80 ± 0.05. KISS1 protein expression in MDA-MB-231 cells increased to 1.35 ± 0.06 at K10 and 1.68 ± 0.08 at K50, while KISS1R increased to 1.30 ± 0.06 and 1.62 ± 0.07, respectively.

In MDA-MB-468 cells, KISS1 increased to 1.02 ± 0.06 at K10 and 1.05 ± 0.07 at K50, whereas KISS1R increased to 1.08 ± 0.06 and 1.10 ± 0.07.

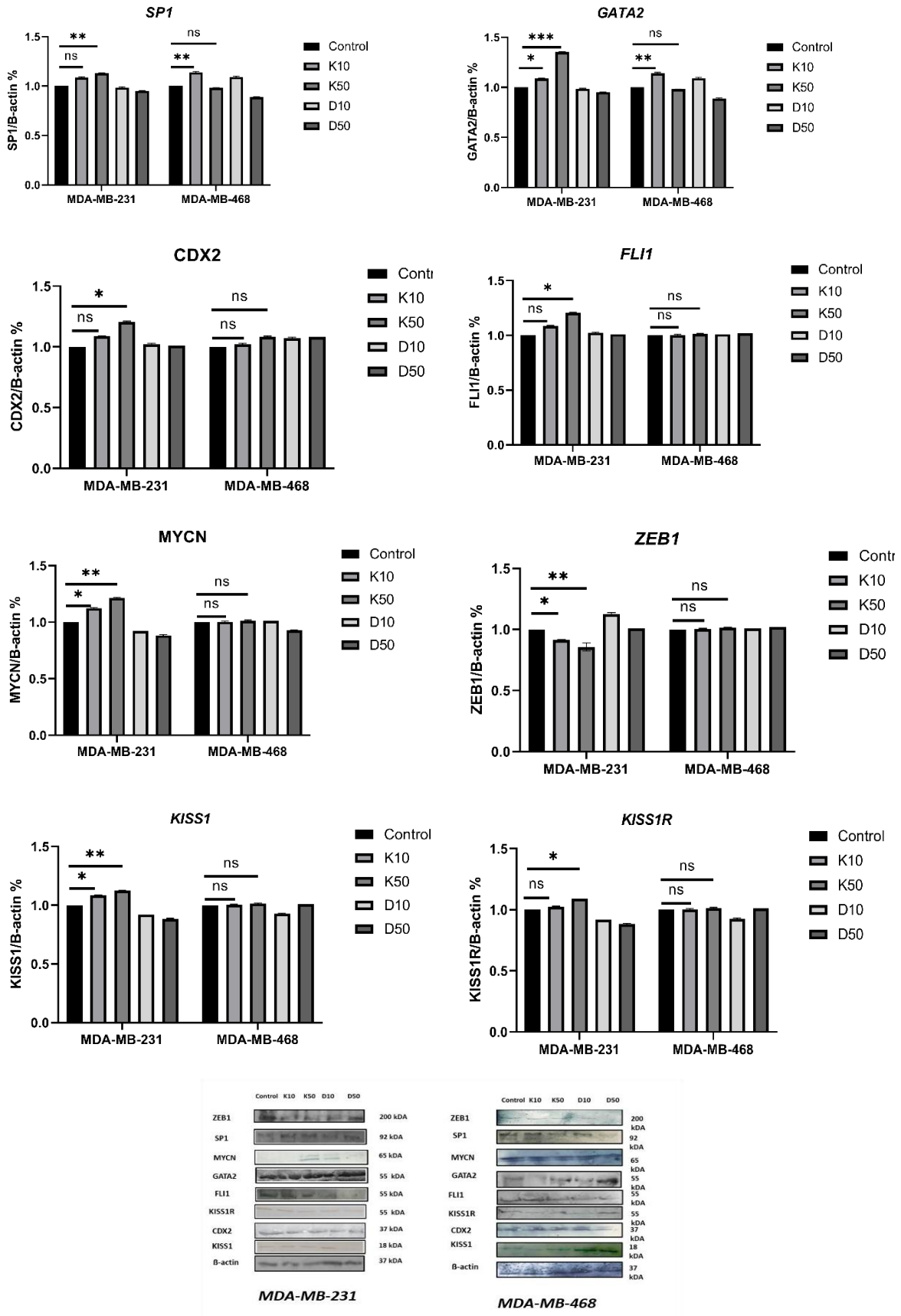

Figure 2.17 a): *Western Blot Analysis of Control vs Kisspeptin-10 treated groups for both the cell line for transcription factors.*

2.4.7.2 Signaling Pathway Proteins

In MDA-MB-231 cells, PKA significantly increased at 1.30 ± 0.06 (K10) and 1.55 ± 0.07 (K50), while PLCB1 increased at 1.15 ± 0.05 and 1.30 ± 0.06. CJUN expression meanwhile reduced to 0.90 ± 0.05 at K10 and 0.78 ± 0.04 at K50.

In MDA-MB-468 cells, PKA increased to 1.02 ± 0.06 and 1.04 ± 0.07, PLCB1 to 1.09 ± 0.05 and 1.09 ± 0.06, whereas CJUN decreased to 0.88 ± 0.05 and 0.82 ± 0.04 at K10 and K50 respectively.

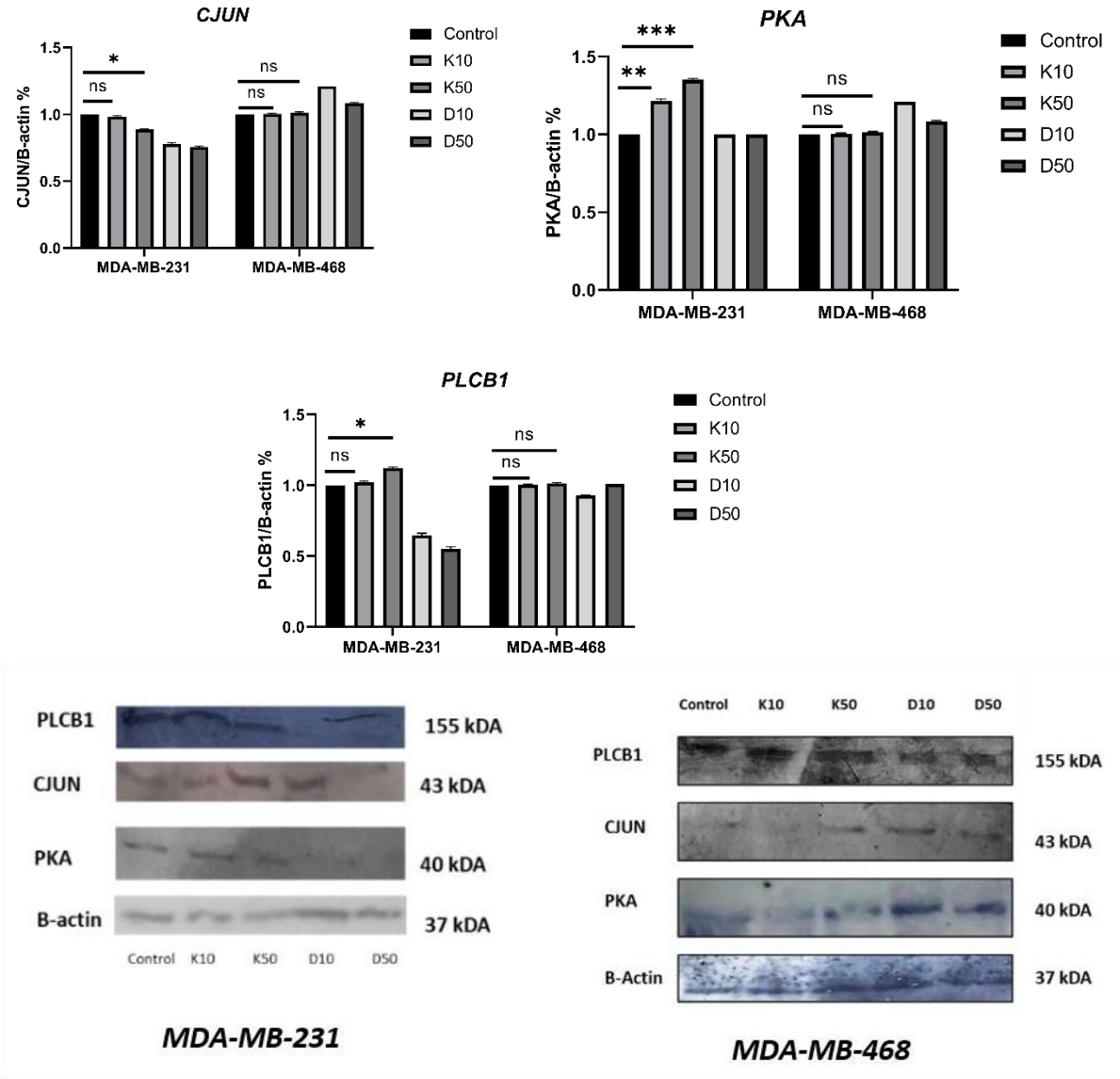

Figure 2.17 b): *Western Blot Analysis of Control vs Kisspeptin-10 treated groups for both the cell line for signalling molecules.*

DISCUSSION

Triple negative breast cancer (TNBC) represents one of the most clinically sinister and biochemically heterogeneous subtypes of breast cancer that remains to be therapeutically targets due to the lack of expression of ER, PR, and Her2 receptors. The complex interplay of aberrant transcriptional regulations, pathway dysregulation of oncogenes, epithelial–mesenchymal transition, apoptotic resistance, and metabolism remains key to the progression and therapeutic resistance of TNBC (Pandey & Pruitt, n.d.). This phenomenological complex microenvironment requires the identification of targets that may play an active role as regulators of multiple oncogenic hallmarks simultaneously for therapeutic efficacy against this triple negative breast cancer microenvironment. With this concept in mind, the current study reveals Kisspeptin10 (KP10), an active endogenous biopeptide encoded by the metastasis inducer gene KISS1, as an active regulator with therapeutic value for TNBC therapy. (Dashti et al., 2020; C. Guo et al., 2025)

Historically, the role of Kisspeptin in breast cancer has been paradoxical. While initially identified as a metastasis suppressor, subsequent studies have reported context-dependent pro-tumorigenic associations, particularly in triple-negative tumors exhibiting elevated KISS1R expression.This duality highlights the importance of investigating Kisspeptin signaling in a controlled experimental framework. Accordingly, our integrated approach combining phenotypic assays, molecular profiling, metabolomics, and *in silico* validation was designed to elucidate the mechanistic basis of KP-10 action in TNBC.(SONG & ZHAO, 2015; Yoon et al., 2023) Our findings demonstrate that KP-10 profoundly reprograms transcription factor networks in MDA-MB-231 cells. Treatment with IC_{10} and IC_{50} doses significantly upregulated SP1, GATA2, CDX2, and MYCN while suppressing ZEB1 and HDAC2. These alterations were consistently validated at both mRNA and protein levels.(Y. Zhang et al., 2019)

Although SP1 is traditionally associated with oncogenic transcription, accumulating evidence indicates that SP1 can mediate differentiation and apoptosis in specific cellular contexts, particularly when regulated by KISS1 signaling. Its KP-10–induced upregulation, coupled with favorable survival outcomes in patient cohorts (HR = 0.62), suggests a tumor-suppressive function in TNBC under Kisspeptin-regulated conditions.(Blake et al., 2017) Similarly, GATA2 and CDX2—both associated with lineage specification and epithelial identity—were significantly induced. GATA2 has been shown to suppress metastasis through chromatin remodeling and stemness regulation, while CDX2 promotes epithelial differentiation and reduces invasive potential in multiple cancers(Cvetković et al., 2013b). Their induction reinforces the concept that KP-10 restores transcriptional fidelity and differentiation-associated programs (Wang et al., 2021b).

Conversely, the repression of ZEB1 and HDAC2 represents a critical mechanistic axis of EMT inhibition. ZEB1 suppresses E-cadherin and activates mesenchymal markers, directly driving

metastasis and therapy resistance (Y. Zhang et al., 2019). HDAC2 promotes chromatin condensation and silencing of tumor suppressor genes, contributing to cellular plasticity and chemoresistance. Their suppression by KP-10 suggests epigenetic relaxation and restoration of epithelial transcriptional programs. Similar EMT-suppressive effects of Kisspeptin have been reported in endometrial and ovarian cancers, supporting the generalizability of this mechanism.(Shan et al., 2017)

Clinical validation using UALCAN confirmed that KP-10–upregulated genes (SP1, GATA2, CDX2, FLI1) are underexpressed in TNBC tumors, whereas KP-10–suppressed genes (ZEB1, HDAC2, MYCN) are overexpressed (Shan et al., 2017). Prognostic analysis further demonstrated that GATA2, SP1, and FLI1 correlate with improved survival, while HDAC2 and MYCN predict poorer outcomes. Collectively, these findings support a model in which KP-10 restores transcriptional homeostasis in TNBC by activating differentiation-associated transcription factors while repressing pro-metastatic and chromatin-condensing regulators.(Silverman et al., 2021; Tang et al., 2017)

KP-10 exposure resulted in significant anti-migratory effects, as demonstrated by wound healing assays. Both IC_{10} and IC_{50} treatments delayed wound closure, with maximal inhibition at IC_{50}. These findings are consistent with Kisspeptin's established anti-metastatic role via KISS1/GPR54-mediated cytoskeletal and adhesion modulation.(H. Yu et al., 2025) Transcriptional profiling revealed dose-dependent upregulation of CDH1 and downregulation of CDH2, CD44, and VIM. Restoration of E-cadherin reinforces epithelial integrity, while suppression of N-cadherin and Vimentin limits cytoskeletal plasticity and migratory competence. CD44 downregulation further suggests impaired cancer stem cell–like behavior. Together, these results confirm that KP-10 induces a mesenchymal-to-epithelial transition (MET), a key event in metastasis suppression. KP-10 robustly activated apoptotic machinery, as evidenced by increased expression of CASPASE-9, CASPASE-3, CASPASE-8, and BAX, along with suppression of BCL2. Caspase-9, a mitochondrial apoptosis initiator, exhibited the strongest induction, indicating dominant activation of intrinsic apoptotic pathways. Caspase-3 upregulation confirmed execution-phase commitment, while Caspase-8 indicated extrinsic pathway contribution(Carneiro & El-Deiry, 2020; Mustafa et al., 2024).

Survival analysis revealed that CASP9 and BCL2 expression correlated with improved patient survival, whereas CASP3 paradoxically correlated with poorer prognosis, likely reflecting compensatory overexpression in aggressive tumors rather than therapeutic induction. Nonetheless, the coordinated caspase activation observed in KP-10–treated cells strongly supports effective apoptotic commitment. (Castro-Piedras et al., 2020; Falco et al., 2021). KP-10 exerted pleiotropic effects on TNBC signaling networks. CJUN, a MAPK/JNK downstream effector, was suppressed at high doses, indicating inhibition of inflammatory and proliferative AP-1 signaling. Although CJUN did not exhibit strong prognostic value, its suppression remains mechanistically relevant.

PKA was significantly upregulated, suggesting activation of the cAMP/PKA axis. PKA is known to inhibit Raf-1 and suppress MAPK signaling, providing a mechanistic basis for reduced proliferation and enhanced apoptosis. PKR (EIF2AK2) was also induced, activating integrated stress response signaling and translational repression. Although high EIF2AK2 correlates with poorer prognosis clinically, its *in vitro* induction likely reflects stress-mediated apoptotic priming. PLCB1 showed modest induction, indicating altered calcium and PKC signaling. While its prognostic value remains unclear, its modulation suggests involvement in GPCR-mediated Kisspeptin signaling dynamics.(Castaño et al., 2009; Tng, 2015) Together, these changes demonstrate that KP-10 suppresses oncogenic transcription while activating stress surveillance and differentiation-associated signaling pathways.

Comparative analysis between MDA-MB-231 and MDA-MB-468 revealed subtype-dependent responsiveness. While both cell lines showed KISS1/KISS1R induction, downstream molecular and functional effects were significantly stronger in MDA-MB-231. EMT reversal, apoptosis induction, transcription factor suppression, and signaling modulation were more pronounced in mesenchymal-like MDA-MB-231 cells, suggesting that KP-10 is particularly effective against aggressive TNBC phenotypes (Shah et al., 2025). Metabolomic profiling revealed extensive metabolic remodeling following KP-10 treatment. Exclusive appearance of metabolites such as Gingerdiol/Norcapsaicin, Usambarensine, and S-Prenyl-L-cysteine in treated groups indicates activation of cytotoxic, redox, and anti-inflammatory pathways. Enrichment of glutathione, amino acid, purine, and TCA cycle intermediates demonstrates metabolic normalization and apoptotic readiness.(X. Li et al., 2019) These metabolic alterations align with transcriptional induction of SP1, GATA2, and MYCN, which regulate stress response and antioxidant pathways. Suppression of ZEB1 further aligns with reduced lipid and cytoskeletal remodeling intermediates, reinforcing EMT inhibition. Transcriptomic analysis across public datasets confirmed TNBC-specific gene dysregulation, including loss of epithelial markers and activation of extracellular matrix, immune, and cytoskeletal remodeling pathways. SP1 and ZEB1 emerged as major regulatory hubs, validating experimental observations. GO enrichment revealed disruption of vesicular trafficking, calcium transport, zinc-binding proteins, and enzymatic regulation, highlighting actionable vulnerabilities.(Liska et al., 2022; Ramirez Moreno et al., 2021) Collectively, these data establish KP-10 as a systems-level regulator that integrates transcription factor modulation, miRNA regulation, signaling pathway control, metabolic rewiring, EMT suppression, and apoptosis activation. Rather than acting as a single-pathway inhibitor, KP-10 orchestrates coordinated molecular reprogramming, converting TNBC cells toward a less invasive, more apoptosis-prone, and transcriptionally stabilized phenotype. The concordance between experimental data and patient survival analysis underscores the translational relevance of KP-10–regulated genes.

CONCLUSION

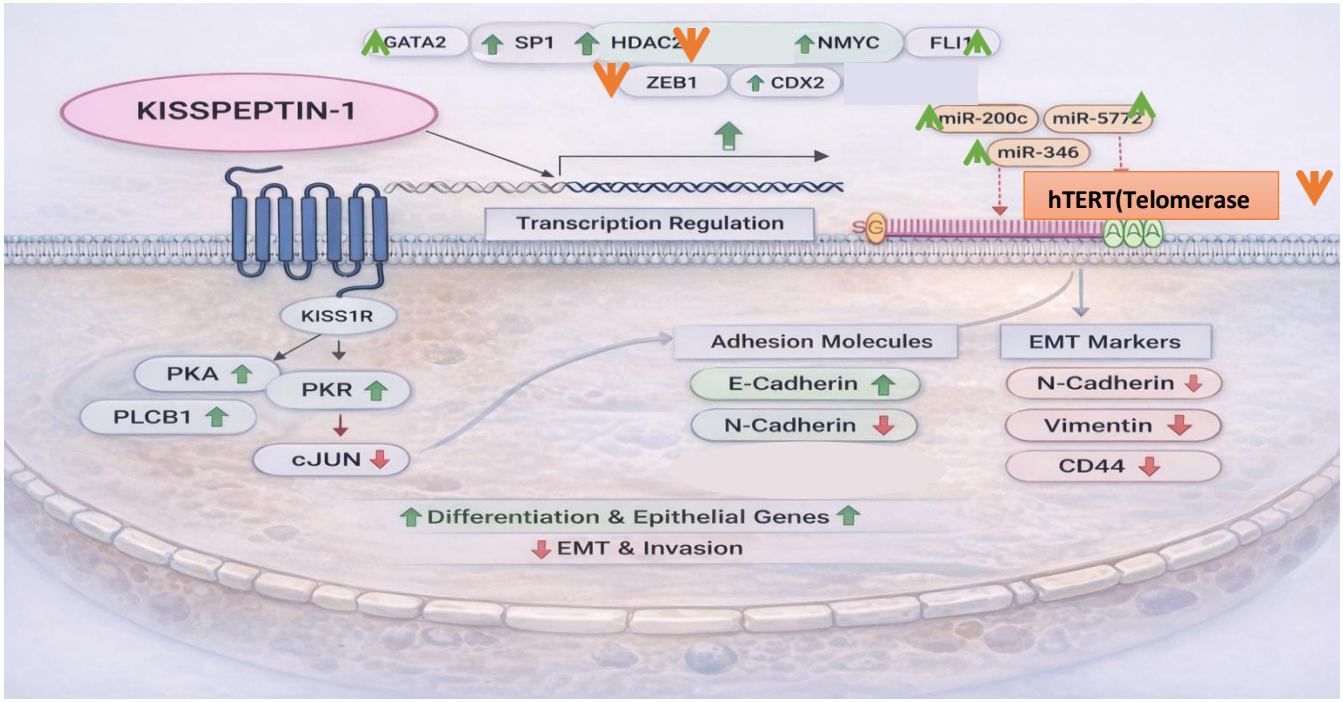

Figure 2.18: *Conclusion Image for the role of Kisspeptin-10 in Triple Negative Breast Cancer*

Exogenous administration of Kisspeptin-10 restores KISS1 expression and exerts multifaceted anti-tumorigenic effects in TNBC cells. Administration of Kisspeptin-10 suppresses cell proliferation, inhibits migration, reverses epithelial-to-mesenchymal transition, and activates intrinsic and extrinsic apoptotic pathways. Moreover, transcriptional and metabolic reprogramming further reinforces a shift toward a less aggressive tumor phenotype. These findings point toward Kisspeptin-10 as one of the potential therapeutic candidates capable of reactivating tumor suppressor networks in TNBC. Following on from this work on triple-negative breast cancer, the next chapter will expand this work to glioblastoma, another aggressive cancer. As all these processes are key to tumor progression, it is important to assess whether Kisspeptin also plays a regulatory role in glioblastoma.